SEISMIC IMAGING OF RECEIVER GHOSTS OF PRIMARIES INSTEAD OF PRIMARIES THEMSELVES

A Thesis

by

NAN MA

Submitted to the Office of Graduate Studies of
Texas A&M University
in partial fulfillment of the requirements for the degree of

MASTER OF SCIENCE

August 2009

Major Subject: Geophysics

SEISMIC IMAGING OF RECEIVER GHOSTS OF PRIMARIES INSTEAD OF PRIMARIES THEMSELVES

A Thesis

by

NAN MA

Submitted to the Office of Graduate Studies of
Texas A&M University
in partial fulfillment of the requirements for the degree of

MASTER OF SCIENCE

Approved by:

Chair of Committee,	Luc T. Ikelle
Committee Members,	Yuefeng Sun
	Daulat D. Mamora
Head of Department,	Andreas Kronenberg

August 2009

Major Subject: Geophysics

ABSTRACT

Seismic Imaging of Receiver Ghosts of Primaries

Instead of Primaries Themselves. (August 2009)

Nan Ma, B.S., China University of Petroleum, Beijing

Chair of Advisory Committee: Dr. Luc T. Ikelle

The three key steps of modern seismic imaging are (1) multiple attenuation, (2) velocity estimation, and (3) migration. The multiple-attenuation step is essentially designed to remove the energy that has bounces at the free surface (also known as "multiples"), since velocity estimation and migration assume that data contain only primaries (i.e., seismic events that have reflected or diffracted only once in the subsurface and have no free-surface reflection). The second step consists of estimating the velocity model such that the migration step can be solved as a linear inverse problem.

This thesis concerns the multiple attenuation of towed-streamer data. We have proposed a new method for attenuating multiples and discussed how this method affects velocity estimation and migration.

The multiple-attenuation approach used today in the E&P industry is based on the scattering theory. It is carried out in two steps: (1) the prediction of multiples using data only, and (2) the subtraction of multiples contained in the data using predicted multiples. One of the interesting features of these multiple-attenuation methods is that they do not require any knowledge of the subsurface. However there are still two drawbacks that

limit the usage of these methods. They are (1) the requirement of acquiring very large 3D datasets which are beyond the capability of current seismic acquisition technology, and (2) the requirement of acquiring near-offset (including zero-offset) data. The method developed in this thesis can potentially overcome these two problems.

The novelty of our approach here is to image receiver ghosts of primaries—events which have one bounce in the subsurface and one bounce at the free-surface that is also the last bounce—instead of primaries themselves. We propose to predict two wavefields instead of a single wavefield, as is presently done. One wavefield contains all free-surface reflections, including receiver ghosts of primaries, ghosts of multiples, and multiples. The other wavefield does not contain receiver ghosts of primaries. We pose the problem of reconstructing receiver ghosts of primaries as solving a system of two equations with three unknowns. The two wavefields are used to construct the two equations. The three unknowns are (1) the receiver ghosts of primaries, (2) the multiples contained in the wavefield containing the receiver ghosts of primaries, and (3) the multiples contained in the other wavefield. We solve this underdetermined system by taking advantage of the fact that seismic data are sparse.

We have validated our approach using data generated by finite-difference modeling (FDM), which is by far the most accurate modeling tool for seismic data. Starting with a simple 1D model, we verified the effectiveness of predicting data containing multiples and receiver ghosts of primaries. Then we used the sparsity of seismic data to turn the system of two equations with three unknowns into a system of two equations with two unknowns on a datapoint basis. We have also validated our method for complex

geological models. The results show that this method is effective, irrespective of the geology. These examples also confirm that our method is not affected by missing near-offset data and does not require special seismic 3D acquisition.

DEDICATION

To my parents, Yanming Ma and Xiaofang Li, may I make you proud.

ACKNOWLEDGEMENTS

I would like to express my gratitude to my academic advisor and committee chair, Dr. Luc T. Ikelle, for his guidance and support in these two years. In particular I would like to thank him for spending his valuable time in guiding me through my research problem.

I would also like to sincerely thank my committee members, Dr. Yuefeng Sun and Dr. Daulat D. Mamora, for their guidance and support throughout the course of this research.

I express my special thanks to all the CASP members for their valuable time and suggestions. Without their help, I would not have been able to complete the thesis on time.

Finally, thanks to my family for their encouragements through my study.

TABLE OF CONTENTS

Page

LIST OF FIGURES

FIGURE Page

CHAPTER I

INTRODUCTION: DEMULTIPLE-BASED ON KIRCHHOFF SCATTERING SERIES

The two widely used marine acquisitions for petroleum exploration and production are: (1) towed-streamer experiments, in which sources and receivers are located near the sea surface; and (2) ocean-bottom-seismic (OBS) experiments, in which the sources are in the water column and the receivers are at the seafloor. About 95% of all marine acquisition today is conducted with the towed-streamer experiment as illustrated in Figure 1.1 (Ikelle and Amundsen, 2005). The method described in this thesis is designed for towed-streamer experiment. We will make a couple of remarks about the ocean-bottom-seismic experiment at the end of Chapter II.

Events in towed-streamer data (Figure 1.2) can be divided into two categories. One category consists of events which include at least one free-surface (sea-surface) reflection in their wavepaths, and the other category consists of events without free-surface reflection in their wavepaths. Events without free-surface reflections are: (1) direct waves (events which do not include any reflection in wavepaths), (2) primaries (events with no free-surface reflection and with reflection only in the subsurface), and (3) internal multiples (events with more than one reflection in the subsurface but not at the free surface). Note that internal multiples in towed-streamer data are generally weak compa-

---

This thesis follows the style and format of Geophysics.

red to primaries, and we will consider them negligible for the purpose of this thesis.

Events with free-surface reflections include ghosts of primaries, free-surface multiples and ghosts of free-surface multiples. Ghosts of primaries are events which have only one free-surface reflection in the wavepaths, and this free-surface refection is either the first reflection to occur in the wavepath of these events (i.e.,the source ghost of primaries) or the last reflection to occur in the wavepath of these events (i.e., the receiver ghost of primaries). All the other events are either free-surface multiples (when the wavepath of events includes one or more free-surface reflections and none is the first or last reflection to occur) or ghosts of free-surface multiples (when the wavepath of events includes two or more free-surface reflections, with either the first or last reflection being a free-surface reflection). Free-surface multiples can be distinguished by the number of bounces at the free-surface. Free-surface multiples that have only one bounce are called first-order free-surface multiples. Second-order free-surface multiples involve two bounces at the free-surface, and so on.

Note that the sources and receivers are very close to the sea surface (less than 5 m) in towed-streamer survey. The receiver ghosts of primaries, which are the particular focus of this thesis, arrive at almost the same time as primaries (see Figure 1.3). Actually, this observation is central to the demultiple algorithm that we will propose in Chapter II.

The modern seismic imaging has three key steps: (1) multiple attenuation; (2) velocity estimation; and (3) migration. We will focus on multiple attenuation (demultiple) as a reconstruction of receiver ghosts of primaries instead of primaries in this thesis and will

discuss the effects of our demultiple approach to velocity estimation and migration in Chapter II.

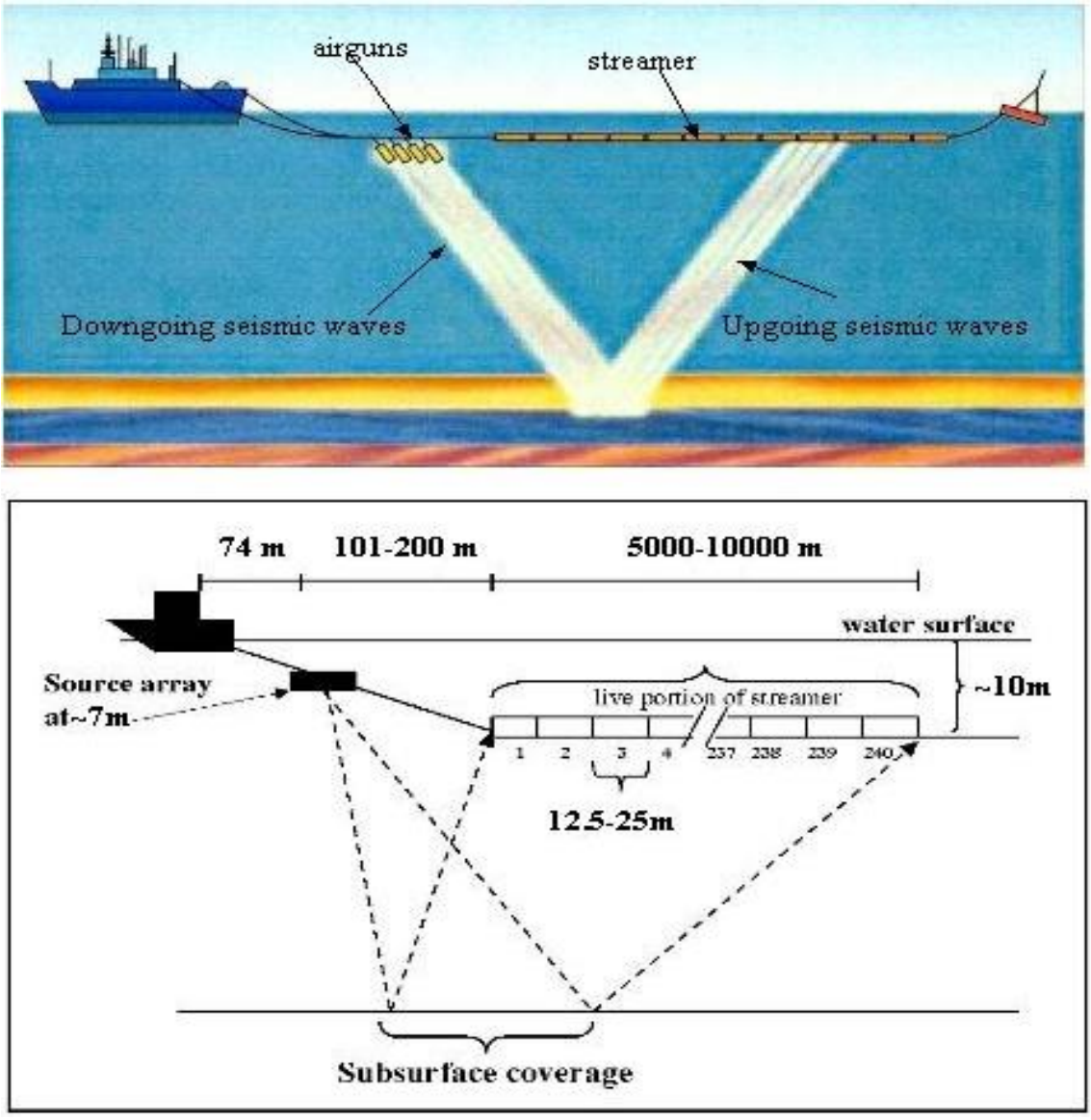

Figure 1.1. Illustration of towed-streamer acquisition. Typical acquisition vessels can tow 12 to 16 streamers spaced 50 m to 100 m apart.

The multiple-attenuation approach used today in the exploration & production industry is based on the scattering theory. In this chapter, we will follow Ikelle et al. (2003) and discuss demultiple technology based on Kirchhoff scattering series. The Kirchhoff scattering series will be described in three sections. We will start by briefly reviewing the construction of multiples based on scattering diagrams. In the second part, we will use the representation theorem to derive Kirchhoff scattering series. The applications of this demultiple method currently have two impediments and we will discuss them at the end of this chapter.

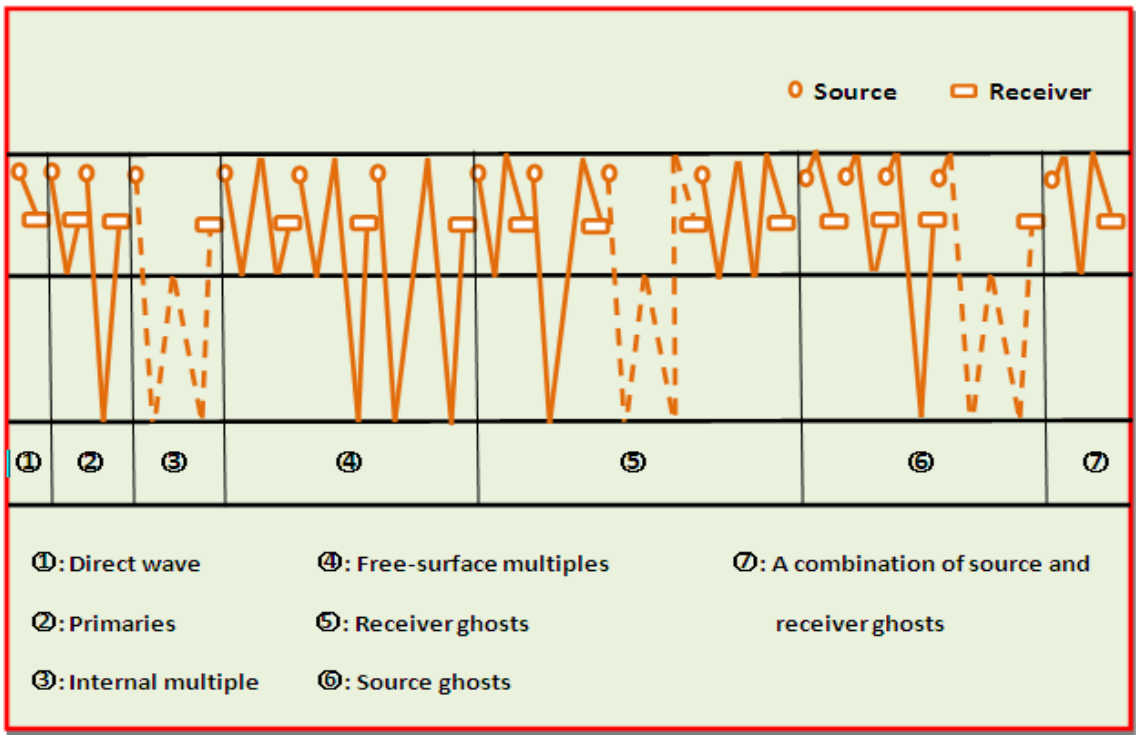

Figure 1.2. Examples of events in towed-streamer data. These events can be grouped into direct waves, primaries, internal multiples, free-surface multiples, receiver ghosts, source ghosts and a combination of source ghosts and receiver ghosts.

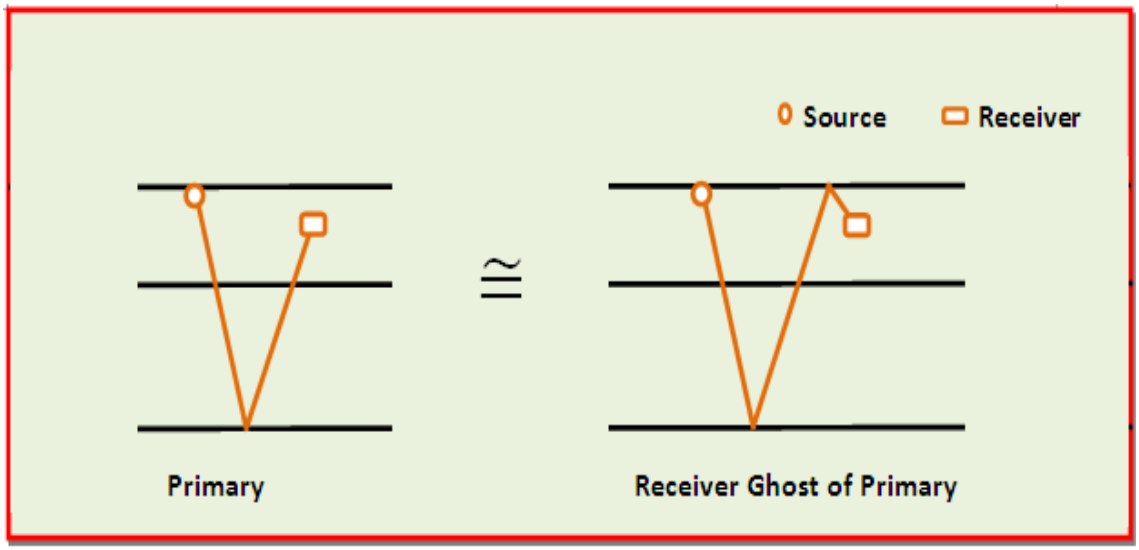

Figure 1.3. Illustration of primaries and receiver ghosts of primaries. In towed-streamer survey, sources and receivers are close to the sea surface. So primaries and receiver ghosts of primaries have almost the same arrivals.

Constructions of Multiples Based on Scattering Diagrams

As illustrated in Figure 1.4, seismic events generally consist of several wavepaths. Each event can be split into two or more events at the scattering point. We can see that seismic events can be described as a combination of two or more events whose connecting point (i.e., scattering point) is either at the sea surface (free surface) or in the subsurface.

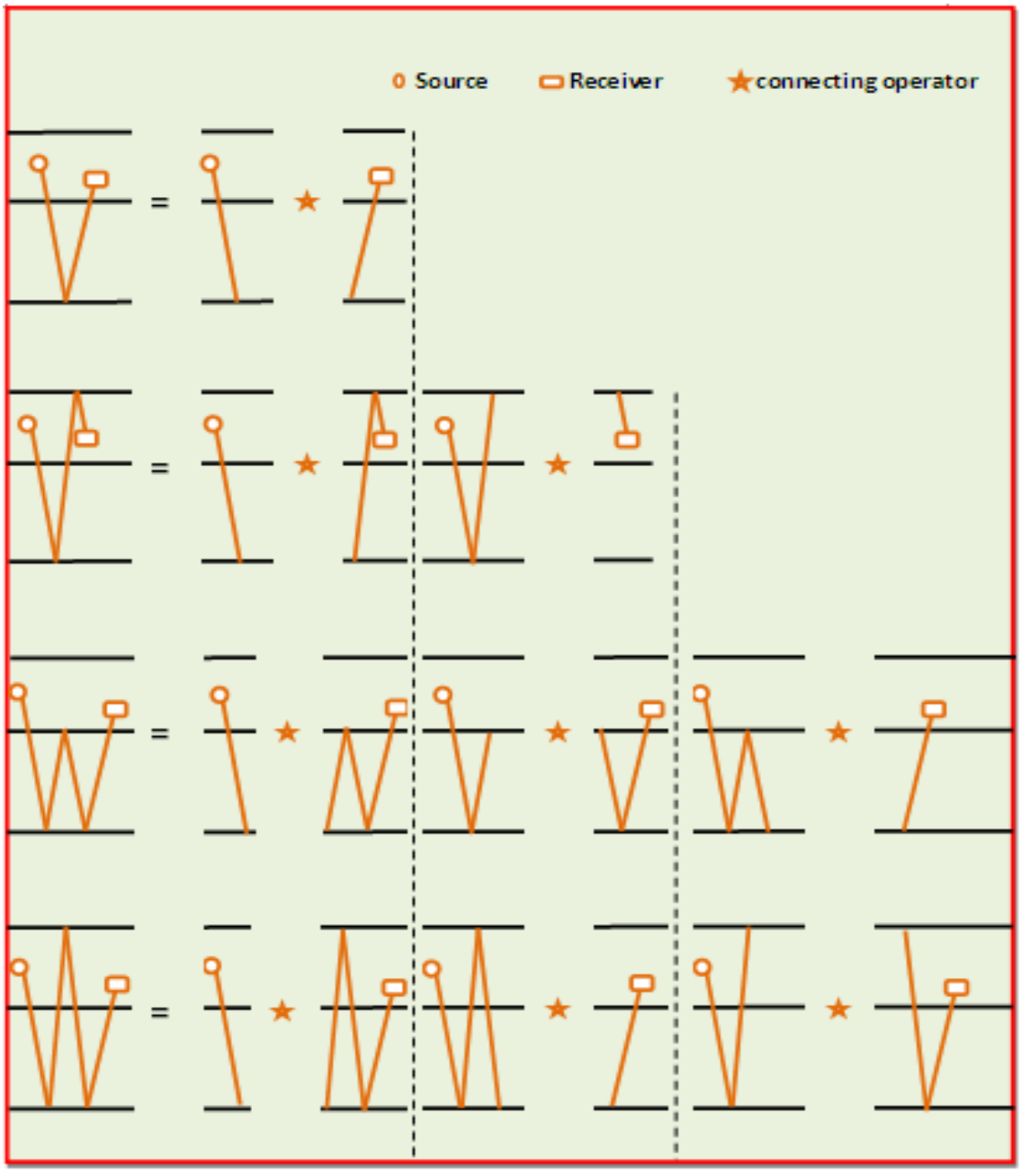

Figure 1.4. Illustration of how seismic events can be constructed. The model used in this illustration consists of a solid layer and a solid half-space overlain by a water layer.

From Figure 1.4, ghosts and free-surface multiples can be constructed with scattering points at free surface or alternatively in the subsurface, whereas primaries and internal multiples can be constructed only with scattering points in the subsurface. Since we do not have receivers in the subsurface, primaries and internal multiples cannot be constructed directly from data recorded at the sea surface. However, ghosts and free-surface multiples have scattering points at the free surface, as we can use recorded data to construct them. In summary, by using only the scattering points located at the free surface, we can construct ghosts and free-surface multiples from seismic data recorded. Therefore, if we are interested in constructing ghosts and free-surface multiples, as we are here, our theory must be constructed for seismic events with scattering points at the free surface.

Let us now concentrate on events with scattering points at the free surface (i.e., on ghosts and free-surface multiples). Figure 1.5 shows a couple of constructions of seismic events. We can see that events with one bounce at the free surface are first-order free-surface multiples and receiver ghosts of primaries. There is only one way of splitting these events with respect to scattering points at the free surface, as illustrated in Figure 1.5. First-order free-surface multiples are constructed as a combination of two primaries. And receiver ghosts of primaries can be constructed as a combination of primary and direct wave.

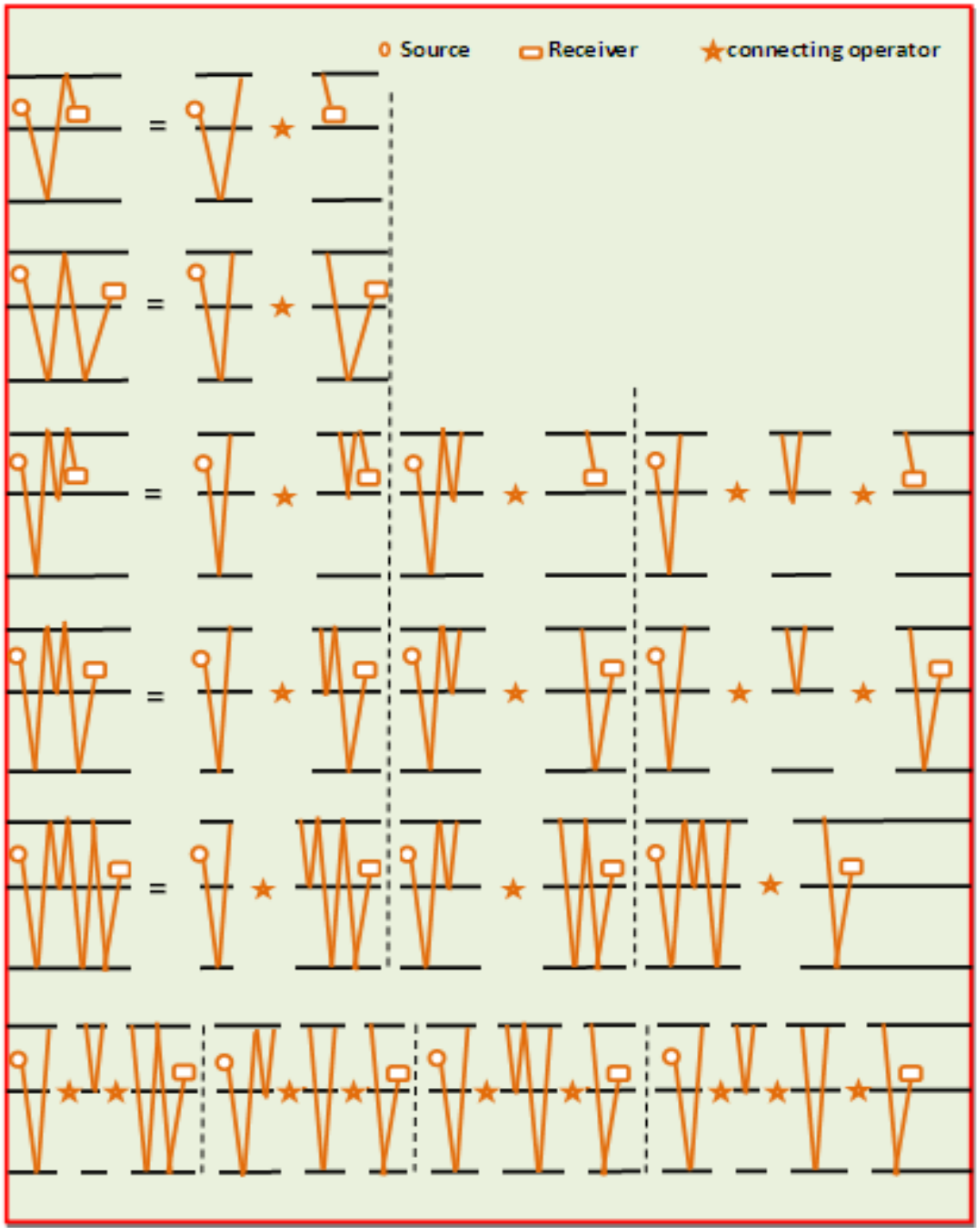

Figure 1.5. Illustration of how ghosts and free-surface multiples can be constructed. The model used in this illustration consists of a solid layer and a solid half-space overlain by a water layer.

As see in Figure 1.5, we can make observations along the same line for higher-order multiples and their ghosts. Here are the summaries of our observations:

1) No primary can be constructed with a scattering point at the free surface.
2) We can construct ghosts of primaries only if the data contain direct wave. Thus, we can eliminate the possibility of constructing ghosts of primaries by muting direct waves from our data results. This point will play an important role in discussing the method in Chapter II.
3) First-order multiples are constructed as a combination of primaries only.
4) Second-order multiples can be constructed as a combination of primaries and first-order multiples with one scattering point. Moreover, with two scattering points, we can also construct second-order multiples as a combination of three primaries.
5) Third-order multiples can be constructed as either a combination of two first-order multiples or as a combination of primary and second-order multiples. Notice that there are three ways to construct third-order multiples with one connecting point, three ways to construct third-order multiples based on two connecting points, and one way to construct third-order multiples based on three interconnections, and so on.

Note that sources and receivers generally are quite close to the sea surface, especially in the towed-streamer experiment considered in the above construction of multiples, as Figure 1.5 suggests. Thus, it is essential to recognize that the data have to be extrapolated from the source to the sea surface or from the receiver to the sea surface.

Derivation of Kirchhoff Scattering Series

The Representation Theorem

We consider a 3D model of the earth consisting of an inhomogeneous solid half-space overlain by a homogeneous fluid (water) layer, as shown in Figure 1.6 (Ikelle and Amundsen, 2005). The position in the configuration is specified by the coordinate $x = (\boldsymbol{x}, z)$, where $\boldsymbol{x} = (x, y)$ represents the horizontal coordinates with respect to a fixed Cartesian referred frame with the origin at O and the three mutually perpendicular base vectors $\{i_1, i_2, i_3\}$. The unit vector i_3 points vertically downward.

We start by rewriting the wave equation that governs the recorded pressure field in the frequency domain. If $p(\boldsymbol{x}, \omega, \boldsymbol{x_s})$ denotes the recorded pressure field for a receiver at $\boldsymbol{x}$ and a point source at $\boldsymbol{x_s}$, it obeys the following equation:

$$L(\mathbf{x}, \omega)p(\boldsymbol{x}, \omega, \boldsymbol{x_s}) = -s(\omega)\delta(\boldsymbol{x} - \boldsymbol{x_s}), \tag{1.1}$$

where

$$L(\mathbf{x}, \omega) = \omega^2 K(\mathbf{x}) + div[\sigma(\mathbf{x})\boldsymbol{grad}], \tag{1.2}$$

with the condition that the pressure field vanishes at the surface (i.e., at the sea surface); that is,

$$p(\boldsymbol{x}, \mathrm{z} = 0, \omega, \boldsymbol{x_s}) = 0, \tag{1.3}$$

where $K(\mathbf{x})$ is the compressibility (the reciprocal of the bulk modulus), $\sigma(\mathbf{x})$ is the specific volume (the reciprocal of density), and $s(\omega)$ is the source signature at point $\boldsymbol{x_s}$.

We also introduce Green's function, which is associated with (1.1) and is denoted by $G(\boldsymbol{x}, \omega; \boldsymbol{x}')$, as follows:

$$L(\mathbf{x}, \omega)G(\boldsymbol{x}, \omega, \boldsymbol{x}') = -\delta(\boldsymbol{x} - \boldsymbol{x}'). \tag{1.4}$$

The boundary conditions for Green's function are not specified here. We will know that we are free to choose the boundary condition in the representation theorem in later discussion.

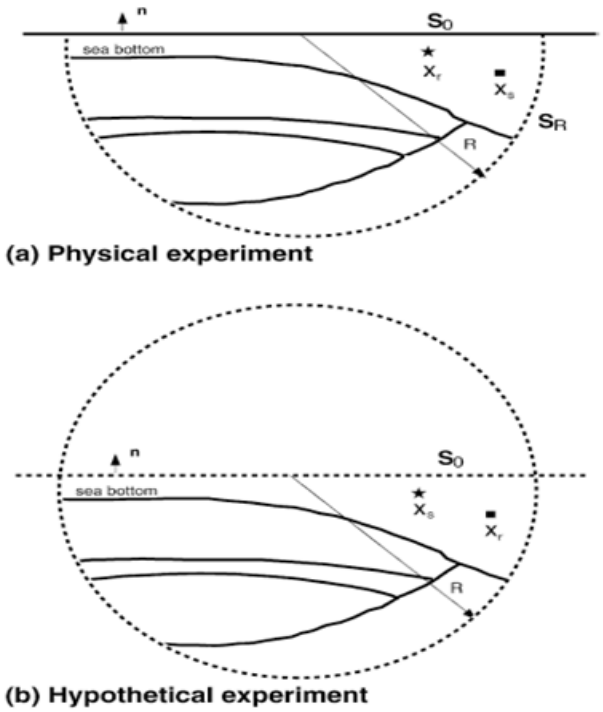

Figure 1.6. Geometry of physical and hypothetical seismic experiments. The surface $\partial D = S_0 + S_R$, with an outward-pointing normal vector **n**, encloses a volume D consisting the water layer and the solid. (a) In the physical experiment, S_0 is a free surface with vanishing pressure. The source is positioned at a center location $\boldsymbol{x_s}$, and the receiver is located at $\boldsymbol{x_r}$. The free surface is a perfect reflector for all upgoing waves, which are reflected downward, thereby giving rise to multiples. (b) In the hypothetical experiment, S_0 is a nonphysical boundary: All upgoing waves from the subsurface continue to propagate in the upward direction. No free surface multiples are generated. The source is a monopole point source located at $\boldsymbol{x_s}$, and the receiver is located at $\boldsymbol{x_r}$.

The representation theorem (Gangi, 1970; Aki and Richards, 1980) is expressed in terms of integrals over surfaces enclosing a volume. The question here is how to reconcile this requirement with our limited towed-streamer measurement along an open surface parallel to the sea surface. Our approach to this question is similar to that of Amundsen (2001), Amundsen et al. (2001), and Ikelle et al. (2003). We consider a volume D enclosed by the surface $\partial D = S_0 + S_R$, with an outward-pointing normal vector **n**, as depicted in Figure 1.6, where S_0 is the air-water surface and S_R represents a hemisphere of radius R. The representation theorem solves for the pressure field inside volume D, assuming that the pressure on surface ∂D, which bounds volume D, is known:

$$p(\boldsymbol{x_r}, \omega, \boldsymbol{x_s}) = G(\boldsymbol{x_r}, \omega, \boldsymbol{x_s}) s(\omega) + \oint_{\partial D} dS(\mathbf{x})\, \sigma(\mathbf{x}) \left[G(\boldsymbol{x}, \omega, \boldsymbol{x_r}) \frac{\partial p(\boldsymbol{x}, \omega, \boldsymbol{x_s})}{\partial n} - p(\boldsymbol{x}, \omega, \boldsymbol{x_s}) \frac{\partial G(\boldsymbol{x}, \omega, \boldsymbol{x_r})}{\partial n} \right]. \quad (1.5)$$

The first term on the right-hand side is included here, because the sources are inside the volume. If we let radius R go to infinity, surface $S_{R\to\infty}$ gives a zero contribution to the surface integral in equation (1.5). This is Sommerfield's (1954) radiation condition. Furthermore, using the boundary conditions (1.3), equation (1.5) becomes

$$p(\boldsymbol{x_r}, \omega, \boldsymbol{x_s}) = G(\boldsymbol{x_r}, \omega, \boldsymbol{x_s}) s(\omega) + \sigma_0 \int_{S_0} dS(\mathbf{x}) G(\boldsymbol{x}, 0, \omega, \boldsymbol{x_r}) \frac{\partial p\left(G(\boldsymbol{x}, 0, \omega, \boldsymbol{x_s})\right)}{\partial n}, \quad (1.6)$$

where $\sigma_0 = \sigma(\boldsymbol{x}, 0)$ is the specific volume in the water. Using the fact that in S_0,

$$\frac{\partial}{\partial n} = -\frac{\partial}{\partial z}, \quad (1.7)$$

and taking the vertical component of the force equilibrium equation, we have the following relationship between the vertical component of the particle velocity and the vertical derivative of the pressure field:

$$i\omega v_z(\boldsymbol{x}, \omega, \boldsymbol{x_s}) = \sigma_0 \frac{\partial p(\boldsymbol{x}, \omega, \boldsymbol{x_s})}{\partial z}. \quad (1.8)$$

Hence, equation (1.6) can also be written as follows:

$$p(\boldsymbol{x_r}, \omega, \boldsymbol{x_s}) = G(\boldsymbol{x_r}, \omega, \boldsymbol{x_s})s(\omega) - i\omega \int_{s_0} dS(\mathbf{x}) G(\boldsymbol{x}, 0, \omega, \boldsymbol{x_r}) v_z(\boldsymbol{x}, 0, \omega, \boldsymbol{x_s}). \quad (1.9)$$

Any Green's function in equation (1.4) can be used in equation (1.9). In other words, we are free to choose boundary for the Green's problem that suits our problem. Thus, we have chosen a Green's function for an infinite medium that has the same 3D homogeneous solid medium as that corresponding to the recorded data and that has an infinite water layer, as described in Figure 1.6b. We will denote it as $G_p(\boldsymbol{x}, \omega, \boldsymbol{x_r})$. Thus, the pressure field containing no free-surface multiples, source ghosts, or receiver ghosts can be written

$$p_p(\boldsymbol{x_r}, \omega, \boldsymbol{x_s}) = G_p(\boldsymbol{x_r}, \omega, \boldsymbol{x_s})s(\omega), \quad (1.10)$$

where $p_p(\boldsymbol{x_r}, \omega, \boldsymbol{x_s})$ denotes data without free-surface multiples and hence with no receiver or source ghosts. Using equation (1.10), equation (1.9) becomes

$$p(\boldsymbol{x_r}, \omega, \boldsymbol{x_s}) = p_p(\boldsymbol{x_r}, \omega, \boldsymbol{x_s}) + a(\omega) \int_{s_0} dS(\mathbf{x})\, p_p(\boldsymbol{x}, 0, \omega, \boldsymbol{x_r}) v_z(\boldsymbol{x}, 0, \omega, \boldsymbol{x_s}). \quad (1.11)$$

where

$$a(\omega) = -\frac{i\omega}{s(\omega)}. \tag{1.12}$$

Equation (1.11) is the desired integral relationship between the pressure field without free-surface multiples $p_p(\boldsymbol{x_r}, \omega, \boldsymbol{x_s})$ and the recorded data $p(\boldsymbol{x_r}, \omega, \boldsymbol{x_s})$ with free-surface multiples.

Let us now interpret equation (1.11) physically, which relates seismic data containing primaries, free-surface multiples, and source and receiver ghosts to data that do not contain these components. The first term on the right-hand side contains primaries and internal multiples. As illustrated in Figure 1.7, the second term (which is a combination of p_p and v_z) predicts all free-surface multiples and receiver and source ghosts. Note that fields p_p and v_z contain direct waves, which allows us to predict receiver and source ghosts of primaries.

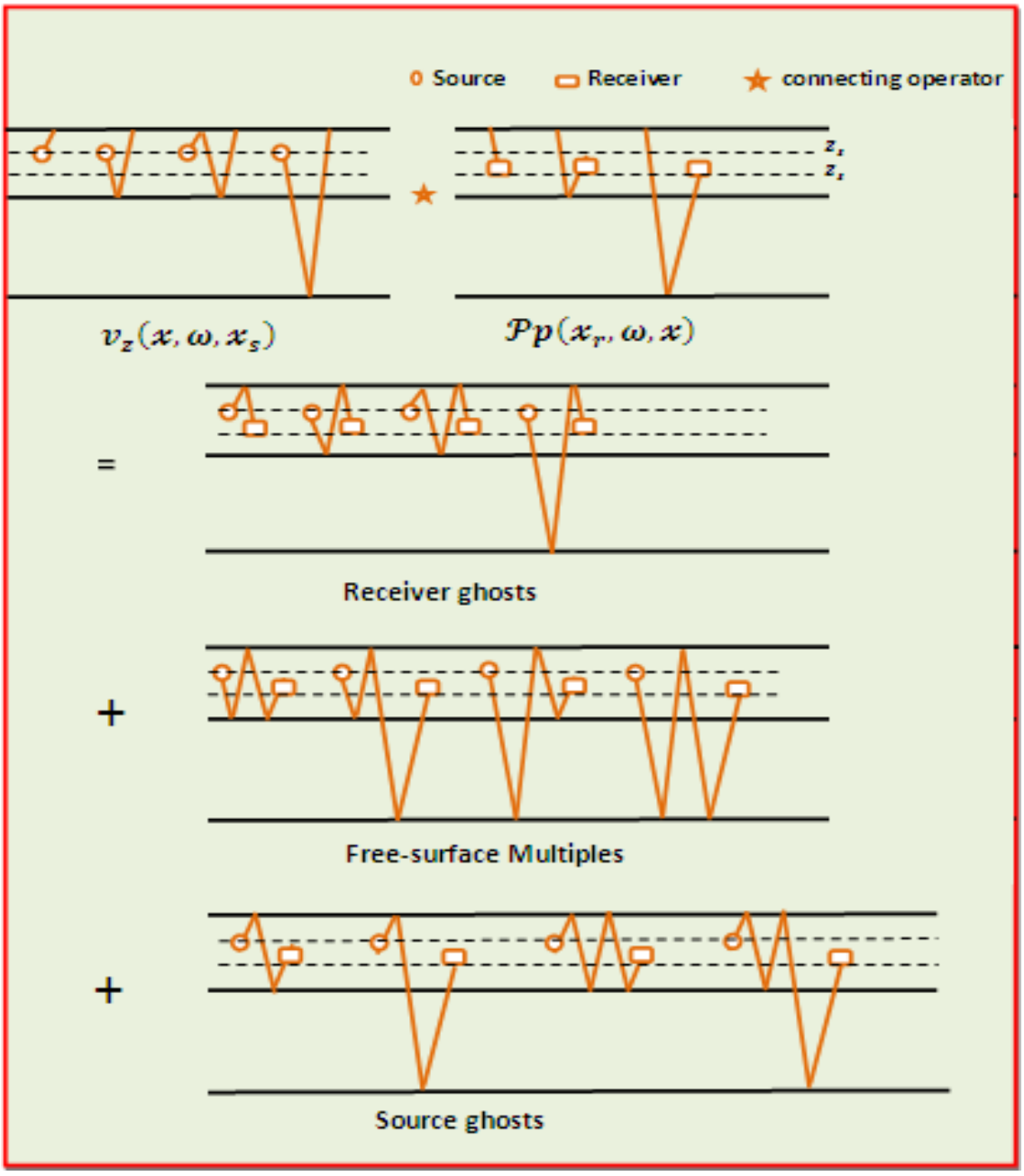

Figure 1.7. Examples of the construction of free-surface multiples and source and receiver ghosts. They can be constructed as a combination of pressure data, containing only primaries with the vertical components of the particle-velocity data; $\mathbf{z}_r$ and $\mathbf{z}_s$ are the depths of the receiver points and shot points, respectively. The symbol * here denotes the multidimensional convolution operations in the second term of equation (1.11), which allows us to combine v_z and p_p.

Extrapolation of the Vertical Component of the Particle Velocity from the Receiver Positions to the Sea Surface

Before we discuss the solution of integral equation (1.11), let us remark that equation (1.11) requires v_z at the free surface s_0. Therefore it is necessary to extrapolate from the actual receiver point $(\boldsymbol{x}, z_r)$ to the point at the free surface $(\boldsymbol{x}, z = 0)$. Similarly, we need to extrapolate the pressure field inside the integral from the source point at the free surface $(\boldsymbol{x}, z = 0)$ to the actual source point $(\boldsymbol{x}, z_s)$.

The particle-velocity field $v_z(\boldsymbol{x}, z_r, \omega, \boldsymbol{x_s})$ consists of an upgoing component $u_v(\boldsymbol{x}, z_r, \omega, \boldsymbol{x_s})$ and a downgoing component $d_v(\boldsymbol{x}, z_r, \omega, \boldsymbol{x_s})$. To get the particle-velocity field at the sea surface, we must forward-extrapolate the upgoing component from $(\boldsymbol{x}, z_r)$ to $(\boldsymbol{x}, z = 0)$ and backward-extrapolate the downgoing component from $(\boldsymbol{x}, z_r)$ to $(\boldsymbol{x}, z = 0)$. These two extrapolated fields must then be recombined to give the total particle-velocity field $v_z(\boldsymbol{x}, z = 0, \omega, \boldsymbol{x_s})$. Because of the free-surface boundary condition at the sea surface, we have

$$u_v(\boldsymbol{x}, z = 0, \omega, \boldsymbol{x_s}) = d_v(\boldsymbol{x}, z = 0, \omega, \boldsymbol{x_s}), \tag{1.13}$$

and because

$$v_z(\boldsymbol{x}, z = 0, \omega, \boldsymbol{x_s}) = u_v(\boldsymbol{x}, z = 0, \omega, \boldsymbol{x_s}) + d_v(\boldsymbol{x}, z = 0, \omega, \boldsymbol{x_s}), \tag{1.14}$$

we get

$$v_z(\boldsymbol{x}, z = 0, \omega, \boldsymbol{x_s}) = 2u_v(\boldsymbol{x}, z = 0, \omega, \boldsymbol{x_s}) = 2d_v(\boldsymbol{x}, z = 0, \omega, \boldsymbol{x_s}). \tag{1.15}$$

Thus, we can get the total particle-velocity field at the sea surface by either forward extrapolating the upgoing component or backward-extrapolating the downgoing component from the receiver location $(\boldsymbol{x}, z_r)$ to location$(\boldsymbol{x}, z = 0)$. We opted to forward-extrapolate the upgoing component.

Because we assume a dual measurement of a pressure field and its vertical derivative, we can use the Osen et al. (1999) formula to obtain the upgoing vertical particle velocity field; that is,

$$U_v(\boldsymbol{k}, z_r, \omega, \boldsymbol{x_s}) = \frac{1}{2}\left[V_z(\boldsymbol{k}, \mathrm{z_r}, \omega, \boldsymbol{x_s}) - \sigma_0 \frac{\kappa_z}{\omega} \mathrm{P}(\boldsymbol{k}, z_r, \omega, \boldsymbol{x_s})\right], \tag{1.16}$$

with

$$k_z = \sqrt{\frac{\omega^2}{c^2} - k_x^2 - k_y^2}, \tag{1.17}$$

where $\boldsymbol{k} = (\mathrm{k_x}, \mathrm{k_y})$ represents the wavenumbers for the horizontal coordinates $\boldsymbol{x} = (x, y)$, and where $V_z(\boldsymbol{k}, z_r, \omega, \boldsymbol{x_s})$ and $\mathrm{P}(\boldsymbol{k}, z_r, \omega, \boldsymbol{x_s})$ are, respectively, the 2D Fourier transforms of $v_z(\boldsymbol{x}, z_r, \omega, \boldsymbol{x_s})$ and $\mathrm{p}(\boldsymbol{x}, z_r, \omega, \boldsymbol{x_s})$ with respect to $\boldsymbol{x}$. The quantity $U_v(\boldsymbol{k}, z_r, \omega, \boldsymbol{x_s})$ denotes the upgoing wavefield of the vertical particle velocity in the wavenumber domain.

The other field that occurs in the surface integral of equation (1.11) is pressure $\mathcal{P}p(\boldsymbol{x}, 0, \omega, \boldsymbol{x_r})$ corresponding to the case of an infinite water layer. The desired pressure is $\mathcal{P}p(\boldsymbol{x}, z_s, \omega, \boldsymbol{x_r})$, rather than $\mathcal{P}p(\boldsymbol{x}, 0, \omega, \boldsymbol{x_r})$. To get the desired field, we extrapolate the field $\mathcal{P}p(\boldsymbol{x}, z_s, \omega, \boldsymbol{x_r})$ from the source location $(\boldsymbol{x}, z_s)$ to $(\boldsymbol{x}, z = 0)$ with regard to particle velocity, the pressure field $\mathcal{P}p(\boldsymbol{x}, z_s, \omega, \boldsymbol{x_r})$ consists of an upgoing component, $u_P(\boldsymbol{x}, z_s, \omega, \boldsymbol{x_r})$ and a downgoing component $d_v(\boldsymbol{x}, z_r, \omega, \boldsymbol{x_s})$. To get desired

pressure at the sea surface, we forward-extrapolate the upgoing component and backward-extrapolate the downgoing component. However, here we must distinguish between the case in which the source is located above the receiver and that in which the source is below the receiver. If the source lies above the receiver, when the reciprocity theorem is invoked, that is, when,

$$\mathcal{P}p(\boldsymbol{x}, z_s, \omega, \boldsymbol{x_r}) = \mathcal{P}p(\boldsymbol{x_r}, \omega, \boldsymbol{x}, z_s), \tag{1.18}$$

or

$$\mathcal{P}p(\boldsymbol{x}, 0, \omega, \boldsymbol{x_r}) = \mathcal{P}p(\boldsymbol{x_r}, \omega, \boldsymbol{x}, 0), \tag{1.19}$$

the result is a simulated source that lies below a simulated receiver. The complete desired pressure field at the simulated receiver, located at $(\boldsymbol{x}, z_s)$, consists of the sum of the upgoing direct wave and the upgoing response from the subsurface. To get the complete desired pressure field at the level of the sea surface $\mathcal{P}p(\boldsymbol{x}, 0, \omega, \boldsymbol{x_r})$, this sum of the upgoing direct wave and the upgoing response from the subsurface must be forward-extrapolated from $(\boldsymbol{x}, z_s)$ to $(\boldsymbol{x}, z = 0)$. On the other hand, if the source lies below the receiver, when reciprocity is invoked the result is a simulated receiver, located at $(\boldsymbol{x}, z_s)$, which consists of the sum of the downgoing direct wave and the upgoing subsurface response.

To get the complete desired pressure field at the level of the sea surface for this case, the direct wave must be isolated and backward-propagated, and the subsurface response must be isolated and forward-extrapolated from $(\boldsymbol{x}, z_s)$ to $(\boldsymbol{x}, z = 0)$. The result must then be summed to get $\mathcal{P}p(\boldsymbol{x}, 0, \omega, \boldsymbol{x_r})$. The subsequent algebra is identical for both cases; that is, the source is located above or below the receiver, as long as the adequate extrapolation factors are used. In seismic acquisition, sources are commonly located above receivers; therefore the derivations that follow are based on this case.

After some reorganization, equation (1.11) becomes

$$p(\boldsymbol{x_r}, \omega, \boldsymbol{x_s}) = \mathcal{P}p(\boldsymbol{x_r}, \omega, \boldsymbol{x_s}) + a(\omega) \int_{S_0} dS(\mathbf{x})\, \mathcal{P}p(\boldsymbol{x}, z_s, \omega, \boldsymbol{x_r})\, \widetilde{v_z}(\boldsymbol{x}, z_s, \omega, \boldsymbol{x_s}), \quad (1.20)$$

where

$$\widetilde{v_z}(\boldsymbol{x}, z_s, \omega, \boldsymbol{x_s}) = \int_{-\infty}^{+\infty} d\boldsymbol{k}\, U_v(\boldsymbol{k}, z_r, \omega, \boldsymbol{x_s}) \exp\{ik_z(z_s + z_r)\} \exp\{ik\boldsymbol{x}\}, \quad (1.21)$$

and where the term $\exp\{ik_z z_s\}$ is introduced by the extrapolation of the pressure field, p_p, inside the integral in equation (1.20) from the source point at the free surface $(\boldsymbol{x}, z_s = 0)$ to the actual source point $(\boldsymbol{x}, z_s)$, and the term $\exp\{ik_z z_r\}$ is introduced by the extrapolation of the vertical particle velocity field, U_z, from a receiver point $(\boldsymbol{x}, z_r)$ to a point at the free surface. Figure 1.8 illustrates field $\widetilde{v_z}$ and the way it interacts with field p_p to predict free-surface multiples and ghosts.

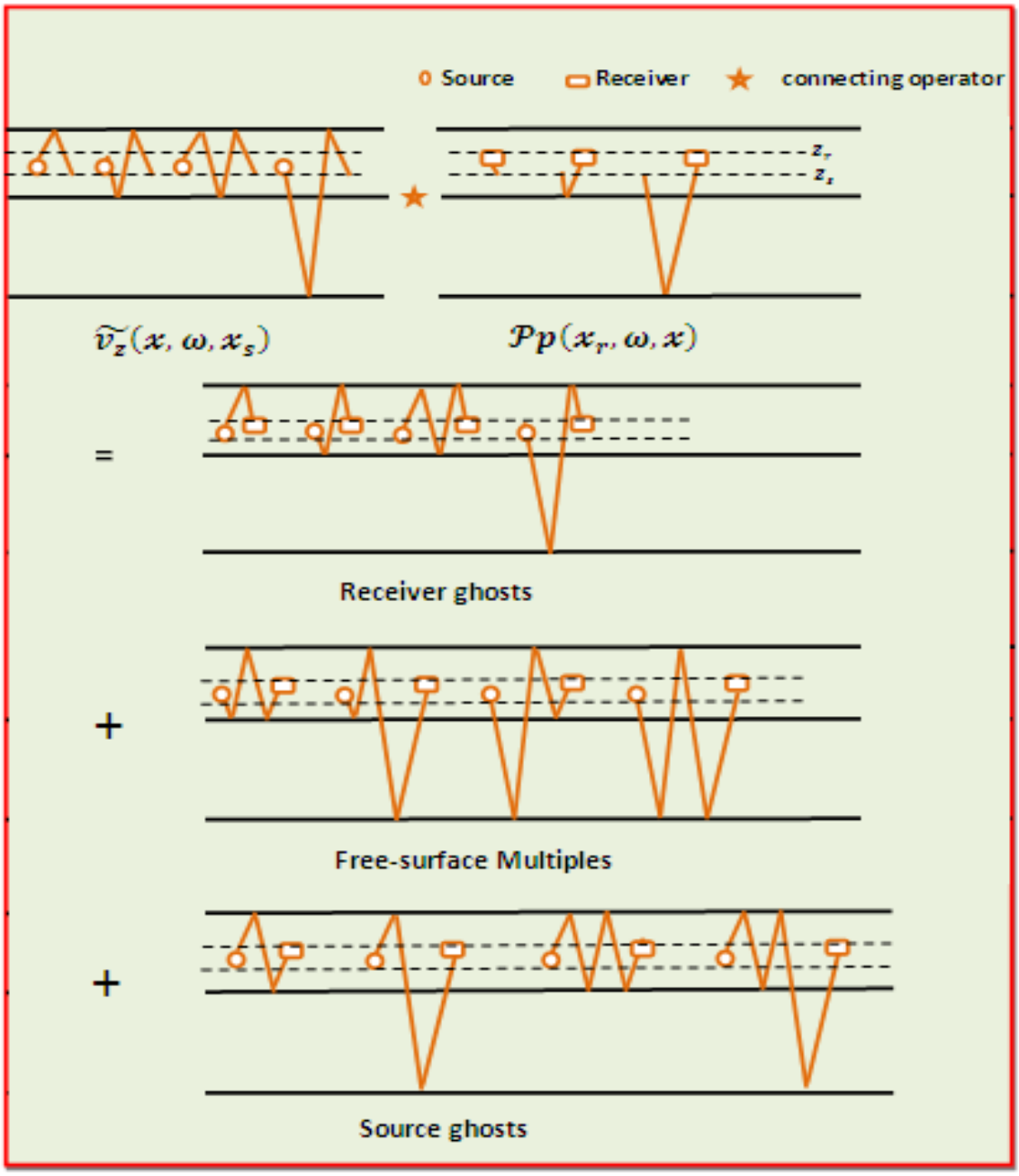

Figure 1.8. Illustration of how the construction of free-surface multiples and source and receiver ghosts in Figure 1.7 is modified when using equation (1.20) instead of (1.11). Notice that the construction of free-surface multiples and ghosts in Figure 1.7 and 1.8 yields the same events, despite their difference.

A Kirchhoff Scattering Series

Assuming that the recorded pressure field, $p_0(\boldsymbol{x_r}, \omega, \boldsymbol{x_s})$ and the recorded vertical component of the particle velocity $\widetilde{v_z}(\boldsymbol{x}, z_s, \omega, \boldsymbol{x_r})$, are available, our next task is to construct the demultiple data $p_p(\boldsymbol{x}, \omega, \boldsymbol{x_s})$, by solving the integral equation (1.20). We propose to solve this integral equation in the form of a series expansion that we will call the Kirchhoff scattering series.

To construct the Kirchhoff scattering series, we start by rewriting equation (1.20) in the form

$$\int_{S_0} dS(\boldsymbol{x}) \{I(\boldsymbol{x}, \boldsymbol{x_s}) + B_{kir}(\boldsymbol{x}, z_s, \omega, \boldsymbol{x_s})\} \times \mathcal{P}p(\boldsymbol{x_r}, \omega, \boldsymbol{x}, z_s) = P_0(\boldsymbol{x_r}, \omega, \boldsymbol{x_s}), \tag{1.22}$$

where

$$B_{kir}(\boldsymbol{x}, z_s, \omega, \boldsymbol{x_s}) = a(\omega)\, \widetilde{v_z}(\boldsymbol{x}, z_s, \omega, \boldsymbol{x_s}), \tag{1.23}$$

and

$$I(\boldsymbol{x}, \boldsymbol{x_s}) = \delta(\boldsymbol{x} - \boldsymbol{x_s}). \tag{1.24}$$

By expanding equation (1.22) as a Taylor series, we arrive at the Kirchhoff scattering series:

$$\mathcal{P}p = P_0 - aP_1 + a^2P_2 - a^3P_3 + \dots, \tag{1.25}$$

with

$$P_n = \widetilde{v_z} P_{n-1}, \quad n = 1, 2, 3, \dots. \tag{1.26}$$

Explicitly, the Kirchhoff scattering series in equation (1.25), which removes free-surface multiples from 3D multi-offset marine data, can be written as follows:

$$\mathcal{P}p(x_r, y_r, z_r, \omega, x_s, y_s, z_s) = P_0(x_r, y_r, z_r, \omega, x_s, y_s, z_s)$$

$$- a(\omega)P_1(x_r, y_r, z_r, \omega, x_s, y_s, z_s) + a^2(\omega)P_2(x_r, y_r, z_r, \omega, x_s, y_s, z_s) - \dots . \quad (1.27)$$

The fields P_1, P_2, etc., are given by

$$P_n(x_r, y_r, z_r, \omega, x_s, y_s, z_s) =$$

$$\int_{-\infty}^{+\infty} dx \int_{-\infty}^{+\infty} dy\, P_{n-1}(x_r, y_r, z_r, \omega, x, y, z_s) \times \widetilde{v_z}(x, y, z_s, \omega, x_s, y_s, z_s). \quad (1.28)$$

Most examples of attenuating free-surface multiples from towed-streamer data are based on equation (1.27). Therefore, it is important to reiterate the different terms of this equation. The term P_0 in equation (1.27) is the actual data that contain primaries, internal multiples, free-surface multiples, and ghosts. The objective of equation (1.27) is to remove free surface multiples and ghosts from P_0. This objective is achieved through computation of the terms P_n in equation (1.28), which allows us to predict multiples. Notice that the computation of P_n must be scaled by $(-a)^n$ to produce the removal of free-surface multiples and ghosts. Because a, as defined in equation (1.12), is the inverse source signature multiplied by a complex constant, we will call a the inverse source signature.

Note that by using the relationship between the vertical component of the particle velocity and the pressure in equation (1.8), we can also derive the Kirchhoff series for the vertical component of the particle velocity.

We have summarized the demultiple process based on the Kirchhoff scattering series as illustrated in Figure 1.9. Basically, using the input data will predict the terms of the Kirchhoff scattering series. Then we estimate the inverse source signature, which can be used to subtract multiples from the data. We have also illustrated this process with

synthetic data in Figure 1.10 (Ikelle and Amundsen, 2005). Note that this process does not require any information of subsurface. We basically have one data set made of three primaries. The second primary and first-order free-surface multiples interfere in the near offset. Yet, we can remove first-order free-surface multiples while preserving primaries despite the interference by using the Kirchhoff scattering series we described above.

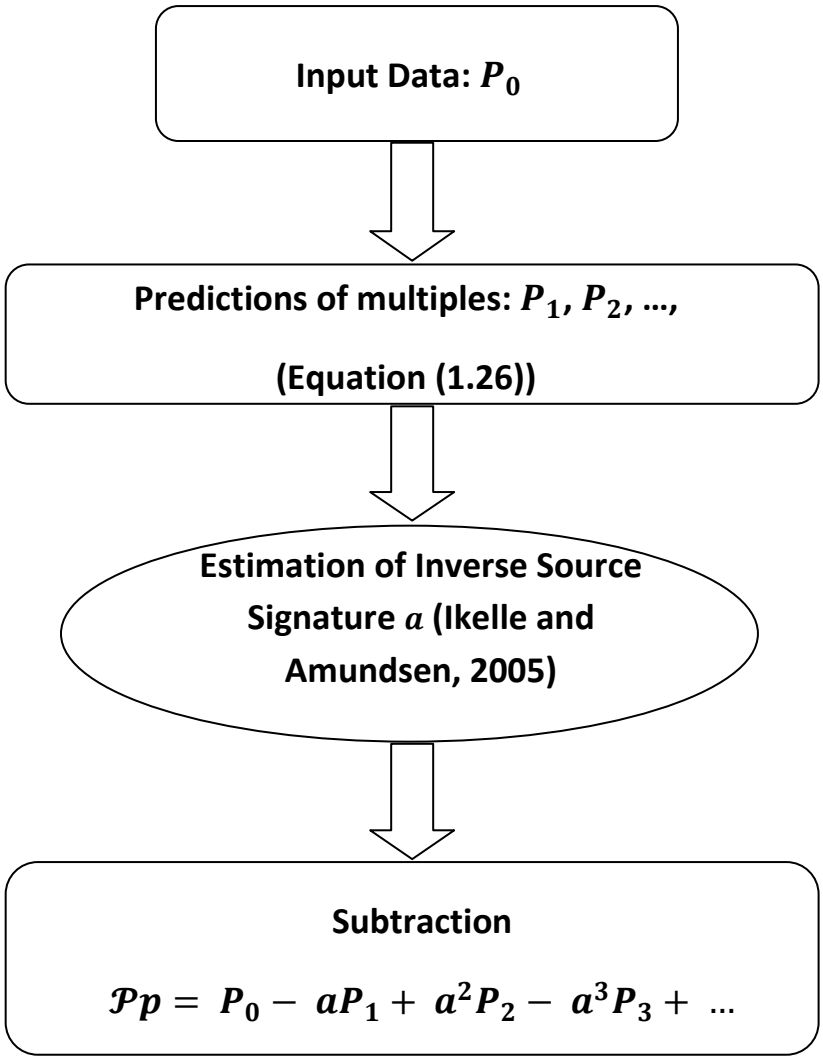

Figure 1.9. Processing flow of a multiple attenuation scheme based on the Kirchhoff scattering series.

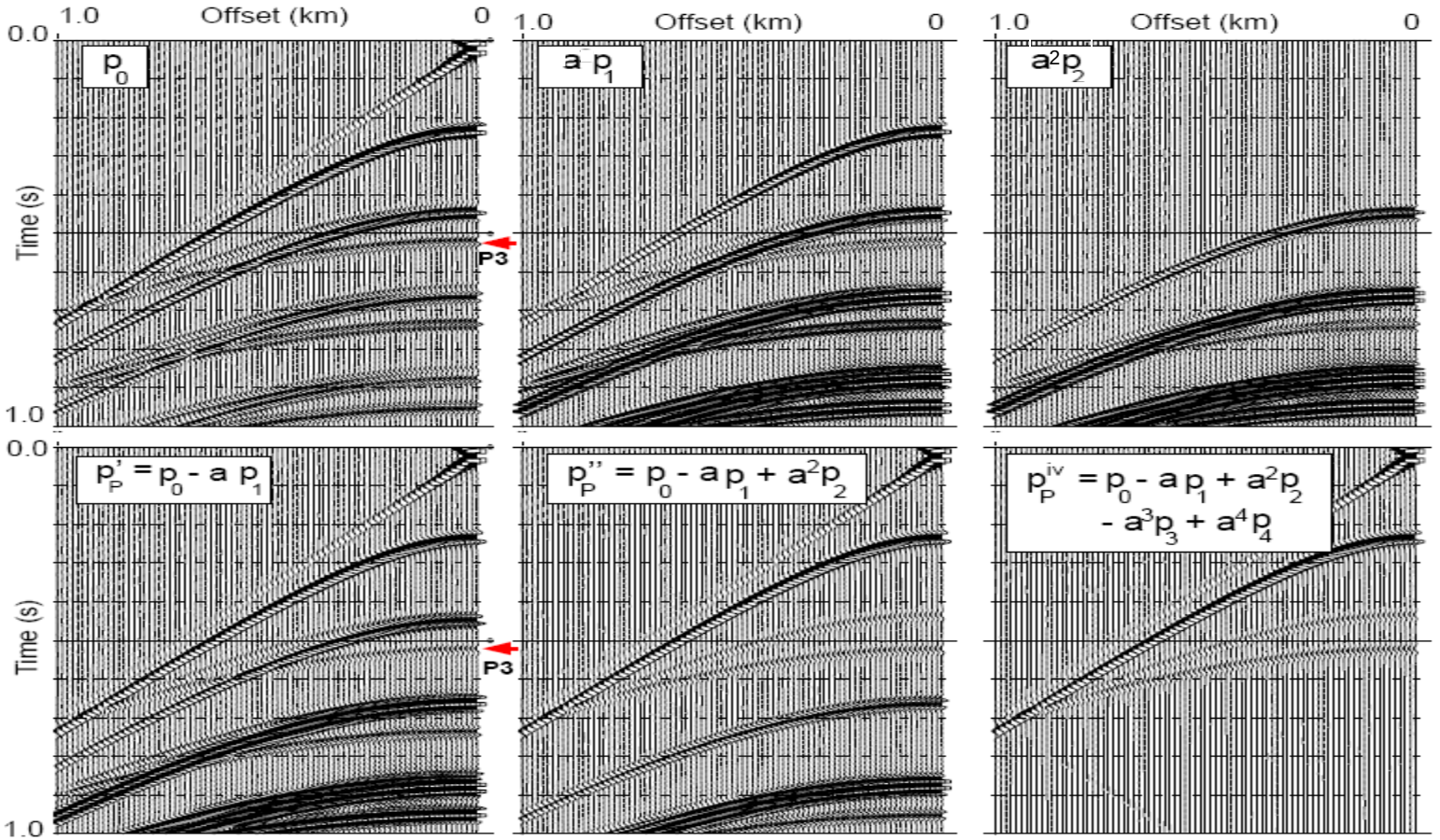

Figure 1.10.Summary of multiple attenuation using the Kirchhoff series derived in equation (1.25). The free-surface multiples are located at about 0.44 s to 1 s. We can see that all multiples contained in P_0 are predicted by P_1. However, when we take the difference between P_0 and aP_1, we can remove only the first-order multiples. Similarly, by adding a^2P_2, we can remove second-order multiples. Here, the multiples are completely removed after adding the forth term of Kirchhoff scattering series.

Problems of Using Kirchhoff Scattering Series

From the description above, we know the Kirchhoff scattering series is effective to remove multiples and does not require any knowledge of subsurface geology. However, there are two important drawbacks which limit the application of Kirchhoff scattering series. They are (1) the requirement of acquiring near-offset (including zero-offset) data and (2) the requirement of acquiring very large 3D datasets that are beyond the capability of current seismic acquisition technology. The objective of this section is to shed more light on these drawbacks.

Extrapolation of Missing Near Traces

In conventional seismic surveys, the nearest offset between the seismic source and the first active receiver ranges from 100 m to 200 m. However, as we see in equation (1.27), the application of the Kirchhoff series requires a complete range of offsets, from zero offset to infinity. The far offsets generally are sufficient for practical implementation of the Kirchhoff series; the problem is the missing near offset. Figure 1.11 gives one example to illustrate the reason why we need to record near offsets up to zero offset when possible, or to interpolate the near offsets from raw data when near offsets are not recorded. For example, to construct a multiple with 250 m, we might need the primaries with 100-m and 150-m offsets. Therefore, in order to predict multiples at 250 m, we need to record 100-m and 150-m offset data which cannot be collected when we choose an

explosive source. One approach to this problem consists of cubic spline fitting of the amplitudes of missing near offsets on NMO-corrected CMP gathers (Verschuur et al., 1992).However, this method does not work for complex geology.

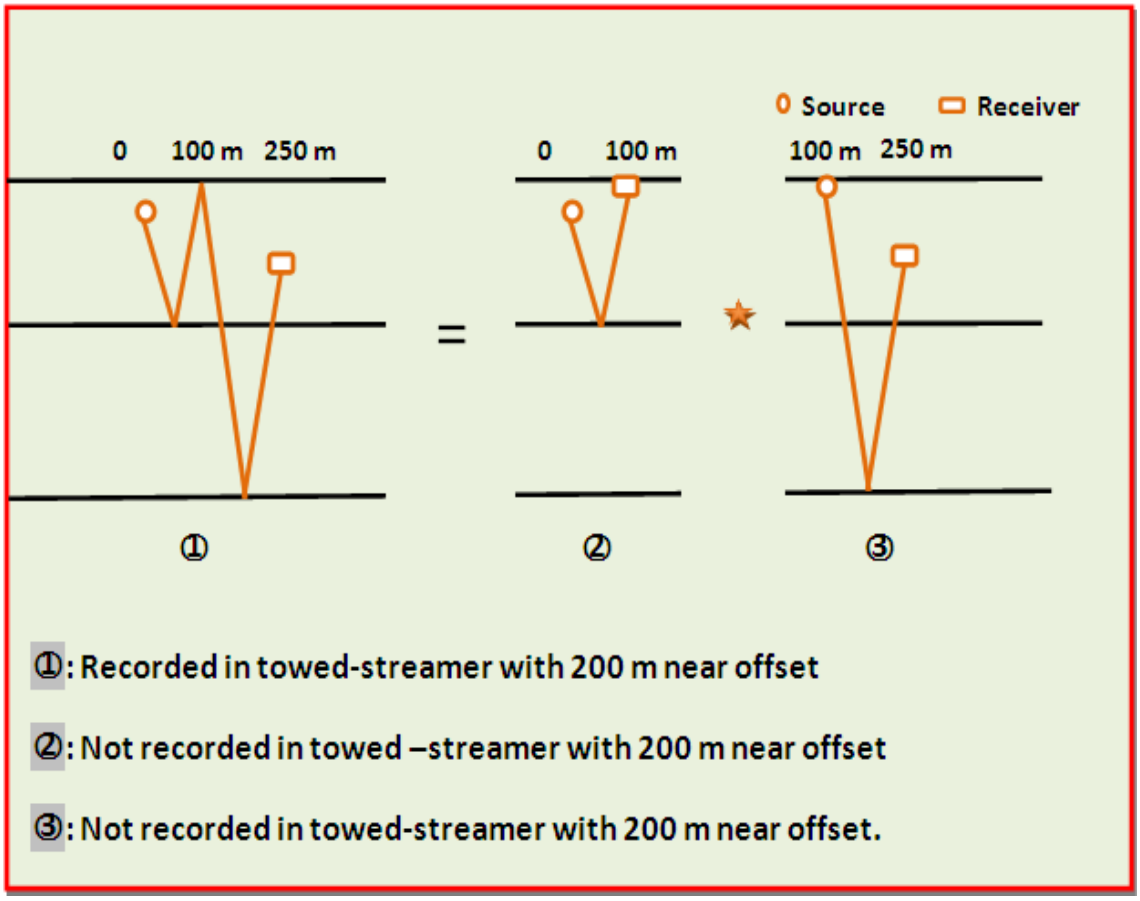

Figure 1.11. Illustration of the reason why we need to record near offsets up to zero offset data when possible.

Surface Integration vs. Line Integration

As defined in equation (1.25), the 3D demultiple algorithm for predicting multiples ($P_1, P_2,$ ...) requires integrals along the x- and y-axes for a pair of source and receiver. In other words, in order to accurately predict multiples for a pair of source and receiver, we need data including all the positions in the surface. Figure 1.12 captures the requirement. Unfortunately, such a requirement is beyond current 3D acquisition, especially towed-streamer experiment. The cables along the y-axis usually have 100 m or more space in real acquisition. One of the major challenges with towed-streamer is to maintain constant streamer spacing. Currents, tides, and other forces can cause streamers to feather, or drift laterally, from the programmed position. In extreme cases, they become tangled. The idea of multiple sweep for a large distance is not economically valuable. These problems will change the travel time of predicted multiples and amplitudes of these multiples. The changes will make our subtraction approach significantly complicated. The method we will describe in Chapter II can potentially overcome these drawbacks.

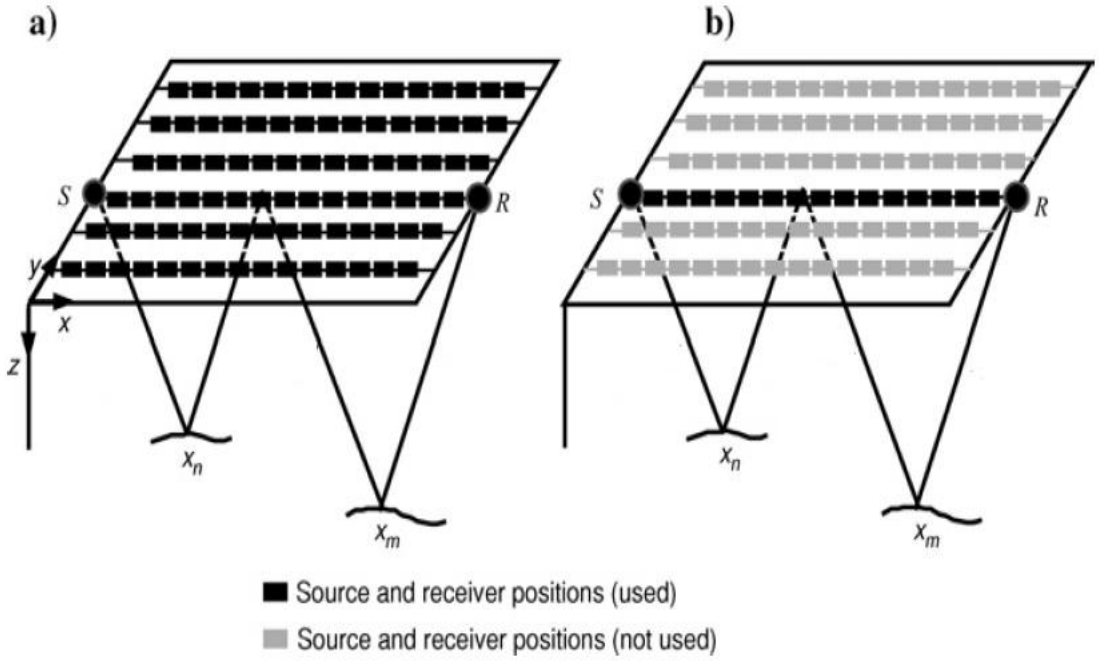

Figure 1.12. Illustration of 2D prediction and 3D prediction. (a) Predicting a multiple between S and R with a 3D demultiple algorithm. In the prediction, all sources and receivers along the x- and y-axes are used. (b) Prediction of a multiple between S and R with a 2D demultiple algorithm. In this prediction, only sources and receivers along x-axis are used.

CHAPTER II

DEMULTIPLE FOR RECEIVER GHOSTS OF PRIMARIES

In the previous chapter, we derived the Kirchhoff scattering series [Equation (1.27)] using the representation theorem. The first term of the Kirchhoff scattering series is the actual data. The second term allows us to predict all events with reflections at the free surface (i.e., ghosts of primaries, free-surface multiples, and ghosts of free-surface multiples). But it can be used only to remove events with one free-surface reflection because events are scaled differently in the Kirchhoff scattering series, in accordance with the number of times they reflect at the free surface. The third term allows us to predict all events with two or more reflections at the free surface. But it aims to attenuate events with two reflections at the free surface, and so on. For example, by using the first three terms of the Kirchhoff scattering series, we can remove events with one and two reflections at the free surface (i.e., receiver ghosts of primaries, first-order free-surface multiples, receiver ghosts of first-order free-surface multiples, and second-order free-surface multiples).

In this chapter, we will present a new way of using the Kirchhoff scattering series for attenuating free-surface multiples which is different from the one we just described. The key characteristic of our approach is that we will try to reconstruct receiver ghosts of primaries instead of primaries themselves. The fact that our demultiple approach will output receiver ghosts of primaries instead of primaries themselves will not affect the

final imaging of the subsurface, because most demultiple algorithms today actually output a combination of primaries and ghosts of primaries.

The basic idea of our method is that we will use the second term of the Kirchhoff scattering series only. In the first case, we will use it with data with direct-wave arrivals. This term allows us to construct receiver ghosts of primaries as well as all the other events with free-surface reflections. In the second case, we will use the second term of the Kirchhoff scattering series with data without direct-wave arrivals. This term no longer predicts receiver ghosts of primaries, but it predicts all the other free-surface reflections. In the first section of this chapter, we will provide the mathematics, scattering diagrams, and numerical examples of these two predictions. In the second and third sections, we will discuss how we can take the differences between these predictions to reconstruct the field containing receiver ghosts of primaries only. Notice that through this chapter, actually throughout the rest of this thesis, we will treat the effect of source ghosts as a part of the seismic source signature.

Basic Formulation of the Demultiple for Receiver Ghosts of Primaries

Let us briefly recall the mathematics of the Kirchhoff scattering series described in Chapter I. Let P_0 represent the pressure towed-streamer data, including direct-wave arrivals, and v_z is the vertical component of the particle velocity of towed-streamer data without direct-wave arrivals. The Kirchhoff scattering series for removing free-surface multiples from pressure towed-streamer data can be written in compact form as follows:

$$\mathcal{P}p = P_0 - aP_1 + a^2P_2 - a^3P_3 + \ldots \quad (2.1)$$

The fields P_1, P_2, etc., are given by

$$P_n = P_{n-1} \times v_z, \quad n \geq 1, \quad (2.2)$$

where the symbol $\times$ denotes the multidimensional convolution operations, $\mathcal{P}p$ is the demultiple pressure data, and a is the inverse source signature.

Here we provide another approach to attenuate free-surface multiples. To facilitate our discussion, we will illustrate each step of our algorithm with numerical examples. Figure 2.1a shows a complex geology (Watts and Ikelle, 2006) that we have used to generate our data. The geology is the deepwater model with two salt bodies. The sources and receivers are located 5 m below the sea surface. We have generated 320 shot gathers spaced every 12.5 m. Each shot gather has 320 receivers. The receivers are also spaced every 12.5 m. Shot points and receiver points share the same positions throughout our survey. We have recorded the pressure data and the vertical component of the particle velocity data simultaneously. Figure 2.1b illustrates one of 320 shot gathers of the raw towed-streamer pressure data P_0. We have used the finite-difference modeling method to generate our data (see Appendix A for the derivation of finite-difference modeling and the conditions of its applicability). This method is by far the most accurate modeling tool for generating seismic data.

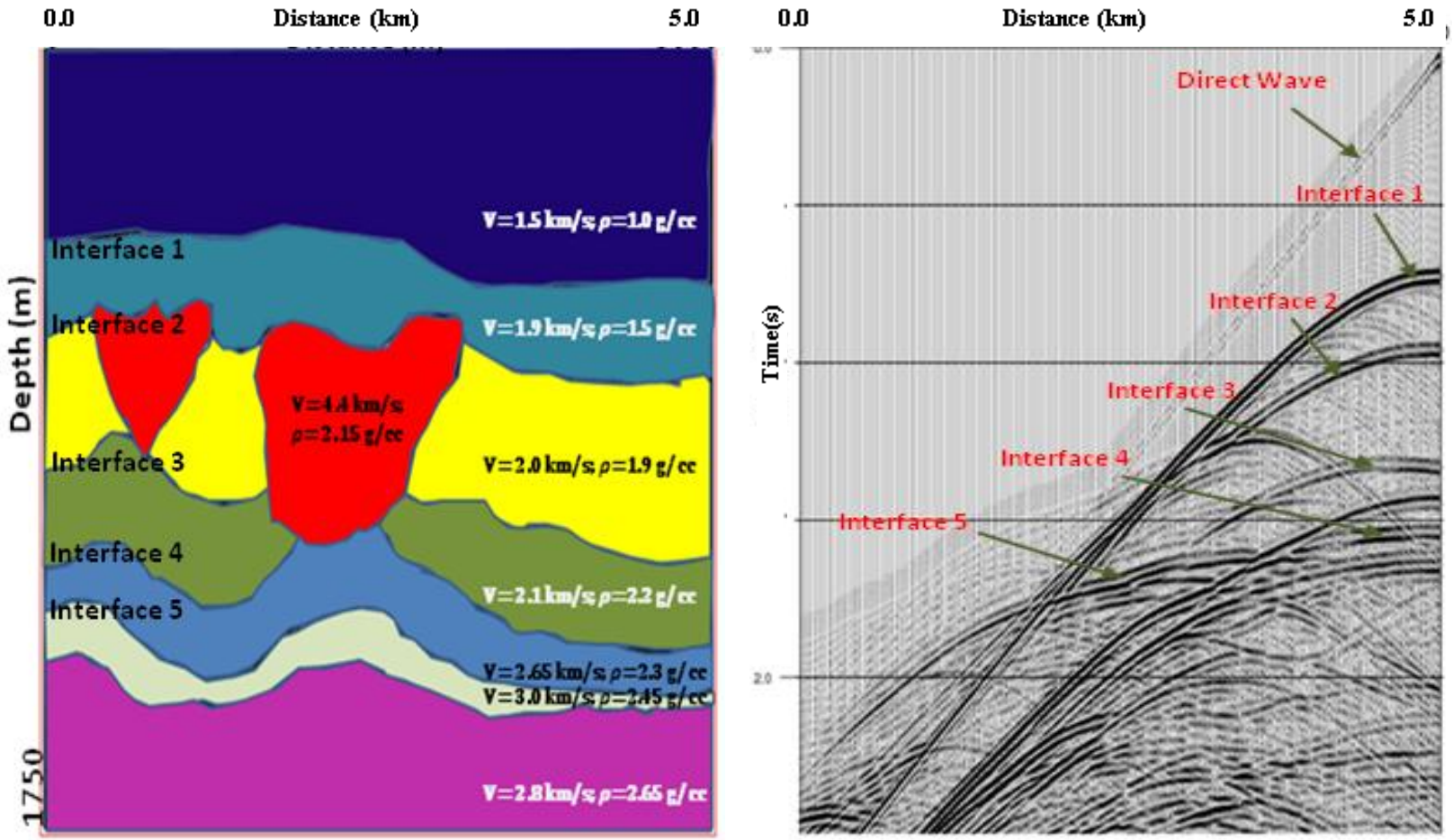

Figure 2.1. Illustration of geology model we will use in this thesis and a shot gather generated from this geology by FDM. (a) A graphical illustration of geology model used in our example. Notice that the geology here is the deepwater model with two salt bodies. (b) Illustration of a shot gather generated from the geology as illustrated in Figure 2.5a by finite-difference modeling method. All the highlighted events are primaries of each interface. Note that direct wave is contained in this figure.

Let us now return to the description of our approach. Our approach is based on the second term of the Kirchhoff scattering series P_1. The basic idea is that P_1 allows us to predict free-surface multiples and receiver ghosts of free-surface multiples as well as receiver ghosts of primaries if P_0 contains direct-wave arrivals. However, if the direct-wave arrivals are removed from P_0, the new P_1, which will be denoted P_1', does not predict receiver ghosts of primaries. Thus the differences between P_1 and P_1', can be used to predict towed-streamer data containing receiver ghosts of primaries only. So our algorithm for recovering receiver ghosts of primaries can be described as follows:

1) Compute P_1 as a multidimensional convolution of the pressure data with the vertical component of the particle velocity as follows:

$$\mathrm{P}_1 = \mathrm{P}_0 \times \mathrm{v}_z, \tag{2.3}$$

where the symbol $\times$ denotes multidimensional convolution operations. Notice that P_0 used in this equation contains direct-wave arrivals.

2) Compute P_1' as a multidimensional convolution of $\mathrm{P}_0^{(\mathrm{nd})}$ with the vertical component of the particle velocity, as follows:

$$\mathrm{P}_1' = \mathrm{P}_0^{(\mathrm{nd})} \times \mathrm{v}_z, \tag{2.4}$$

where $\mathrm{P}_0^{(\mathrm{nd})}$is the actual pressure data without direct-wave arrivals. Notice that in contrast to P_1, P_1' does not predict any receiver ghosts of primaries, as illustrated in Figure 2.2. In Figure 2.2a, the output of the first prediction includes receiver ghosts of primaries, free-surface multiples, and receiver ghosts of free-surface multiples. Figure 2.2b shows that we can predict free-surface multiples and their associated

receiver ghosts if the pressure field does not include direct-wave arrivals. However, the number of times receiver ghosts of free-surface multiples predicted in P_1 is different from the one predicted in P_1'. For example, a receiver ghost of a first-order free-surface multiple can be constructed in two ways: (1) as a multidimensional convolution of a direct wave with a first-order free-surface multiple and (2) as a multidimensional convolution of a primary with a receiver ghost of a primary. Figure 2.3 provides an illustration of these constructions. Notice that P_1 predicts both of these events, while P_1' predicts only one of them. A similar analysis for a receiver ghost of a second-order free-surface multiple shows that P_1 will predict it three times, whereas P_1' can predict only the receiver ghost of a second-order free-surface multiple twice. Hence, P_1 and P_1' contain the same receiver ghosts of free-surface multiples with different multiplicative factors. The need to compensate for these differences is the reason for developing special schemes for our demultiple technique.

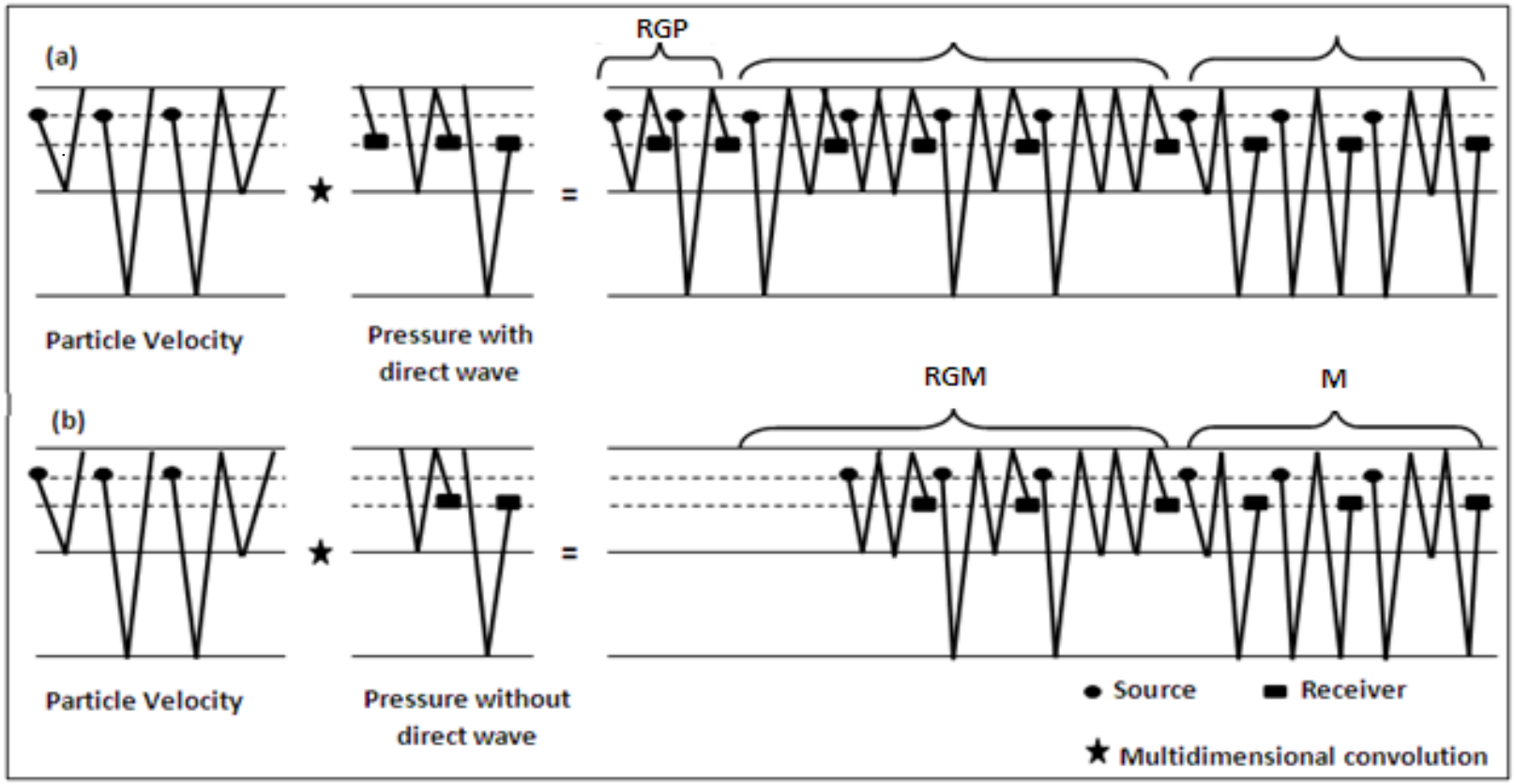

Figure 2.2. The comparison of P_1 and P_1' using scattering diagrams. (a) Illustration of the construction of P_1 in which the pressure field P_0includes direct-wave arrivals. Notice that we have constructed receiver ghosts of primaries, free-surface multiples and receiver ghosts of free-surface multiples. (b) Illustration of the construction of P_1' with $P_0^{(nd)}$. Notice that we have not constructed receiver ghosts of primaries in this case. Also notice that the number of receiver ghosts of free-surface multiples events predicted P_1 and P_1' is different. RGP denotes receiver ghosts of primaries, RGM denotes receiver ghosts of free-surface multiples, and M denotes free-surface multiples.

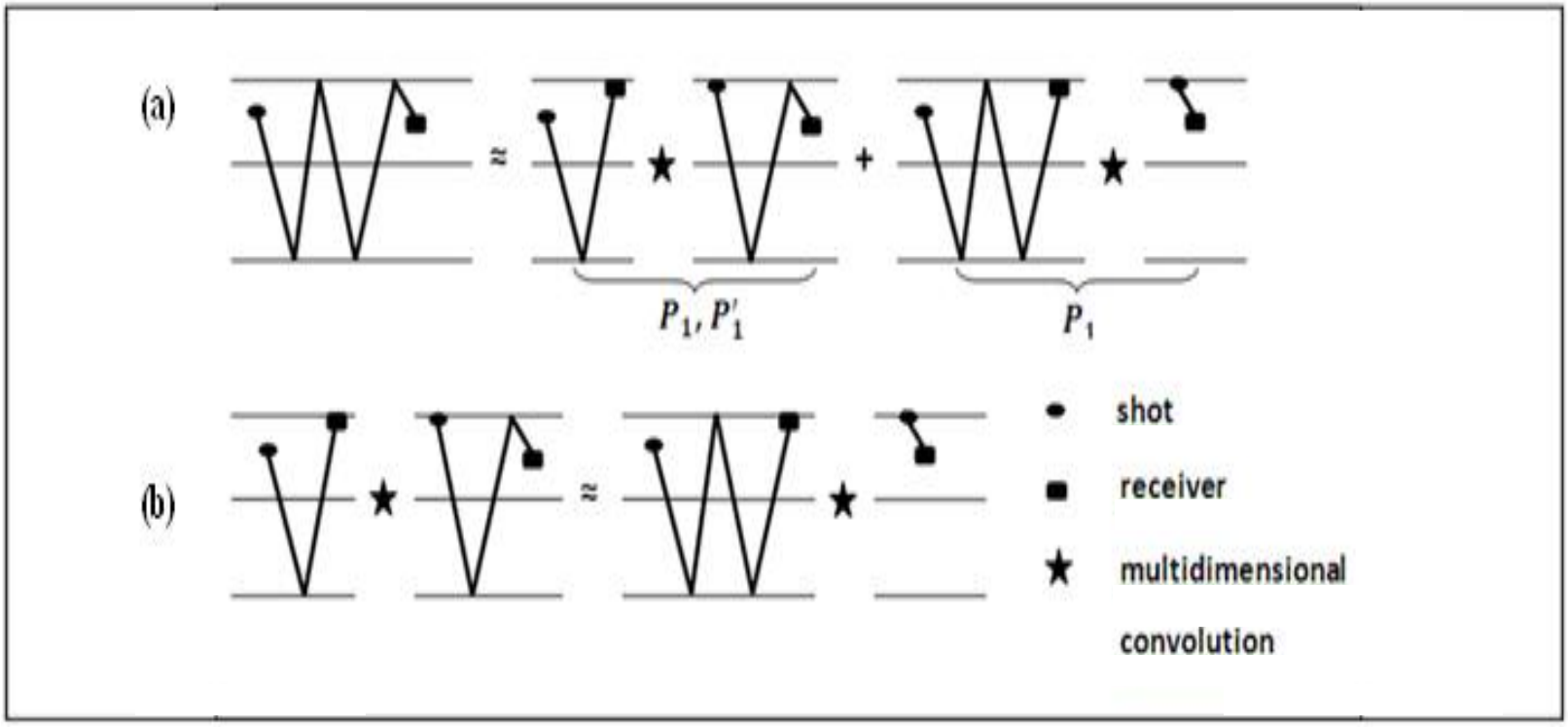

Figure 2.3. Illustration of construction of receiver ghosts of free-surface multiples. (a) The receiver ghosts of free-surface multiples can be constructed as a multidimensional convolution of a multiple with a direct wave, or as a multiple (primary) with a receiver ghosts of a multiple (a receiver ghost of primary). Notice the differences in the multiplicative factor between the receiver ghosts of free-surface multiples in P_1 and P_1'. (b) Here we illustrate that the scattering point in the construction of receiver ghosts of multiples in P_1 can be different with the same event constructed in P_1'.

3) We have developed two ways of reconstructing receiver ghosts of primaries from the predicted wavefields P_1 and P_1'. One way is to take the difference between P_1 and P_1' to obtain the field containing only receiver ghosts of primaries if the actual pressure data do contain only first-order free-surface multiples like the data recorded in ultra deepwater. If the data contain more than one order of free-surface multiples, the differences in the multiplicative factor between the receiver ghosts of free-surface multiples in the two predictions do not allow us to subtract all orders of free-surface multiples simultaneously. In this case, we have opted to use the other method. We will describe these two methods in the following two sections.

Before we turn to a discussion of our subtraction schemes, let us illustrate P_1 and P_1' for the data in Figure 2.4a. Notice that we have plotted these data without direct-wave arrivals. These two predictions, P_1 and P_1', are shown in Figure 2.4b and 2.4c, respectively. All events contained in P_0 also present in P_1. Moreover, we can see that the kinematics of P_0 are almost identical to those in P_1. Therefore, we can confirm that receiver ghosts of primaries in P_1 arrive at almost the same time as primaries in P_0, as we pointed out in Figure 1.3. Actually, P_0 and P_1 are also very similar in AVO terms if one can compensate for the fact: (1) that the source signature in P_1 is broader than the one in P_0 and (2) that the geometrical spreading of P_1 has been by convolution with the direct-wave arrivals.

Let us now compare P_1 and P_1'. We can see that P_1' does not contain receiver ghosts of primaries. However, it contains the same multiple events as P_1. Hence, the difference between P_1 and P_1' can allow us to recover receiver ghosts of primaries. The difference in the apparent source signature between P_1 and P_1' is just due to the differences in plotting scales.

Figure 2.5 also illustrates the differences between P_0 , P_1, and P_1'. But this time we have used offset gathers, more precisely zero-offset gathers, to provide a more-comprehensive description of our dataset. The conclusions that we have just made based on the shot gather in Figure 2.4 also hold for the offset gather.

In summary, we have proposed to use the second term of the Kirchhoff scattering series with and without direct-wave arrivals to product two wavefields. One wavefield contains all free-surface reflections, including receiver ghosts of primaries, receiver ghosts of free-surface multiples, and free-surface multiples. The other wavefield does not contain receiver ghosts of primaries. Our challenge in the next two sections is to develop schemes which allow us to recover receiver ghosts of primaries.

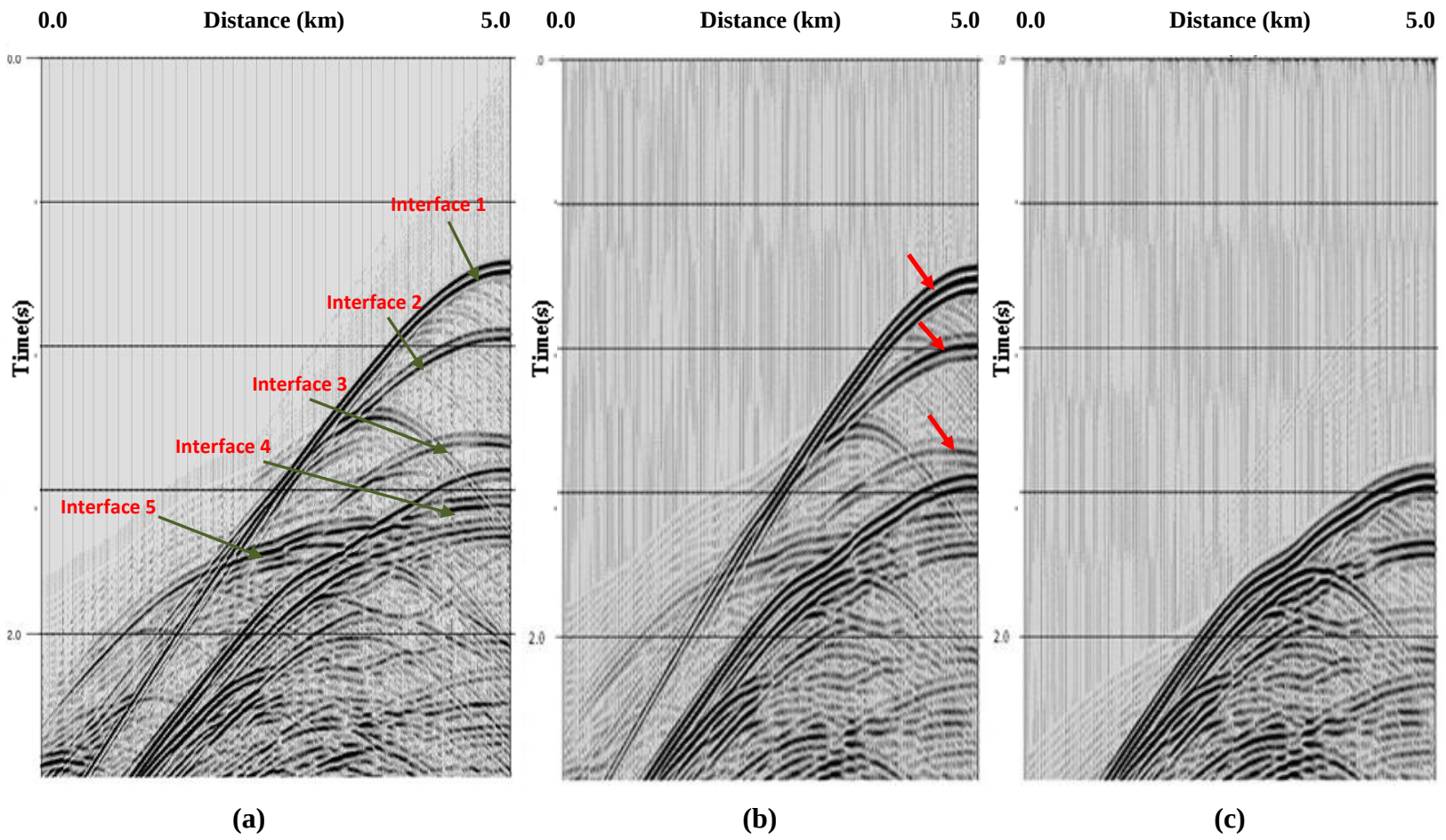

Figure 2.4. Illustration of the two predictions of the shot gather. (a) Illustration of a shot gather of the synthetic data using the geology as illustrated in Figure 2.3a. (b) Illustration of a shot gather from the data generated from FDM. (b) Illustration of the field P_1 after applying Equation (2.3). Note that the receiver ghosts of primaries and primaries in Figure 2.4a have almost the same arrivals. (c) Illustration of the field $P_1^{'}$ after applying Equation (2.4). Notice that Figure 2.4b contains all the events in this figure.

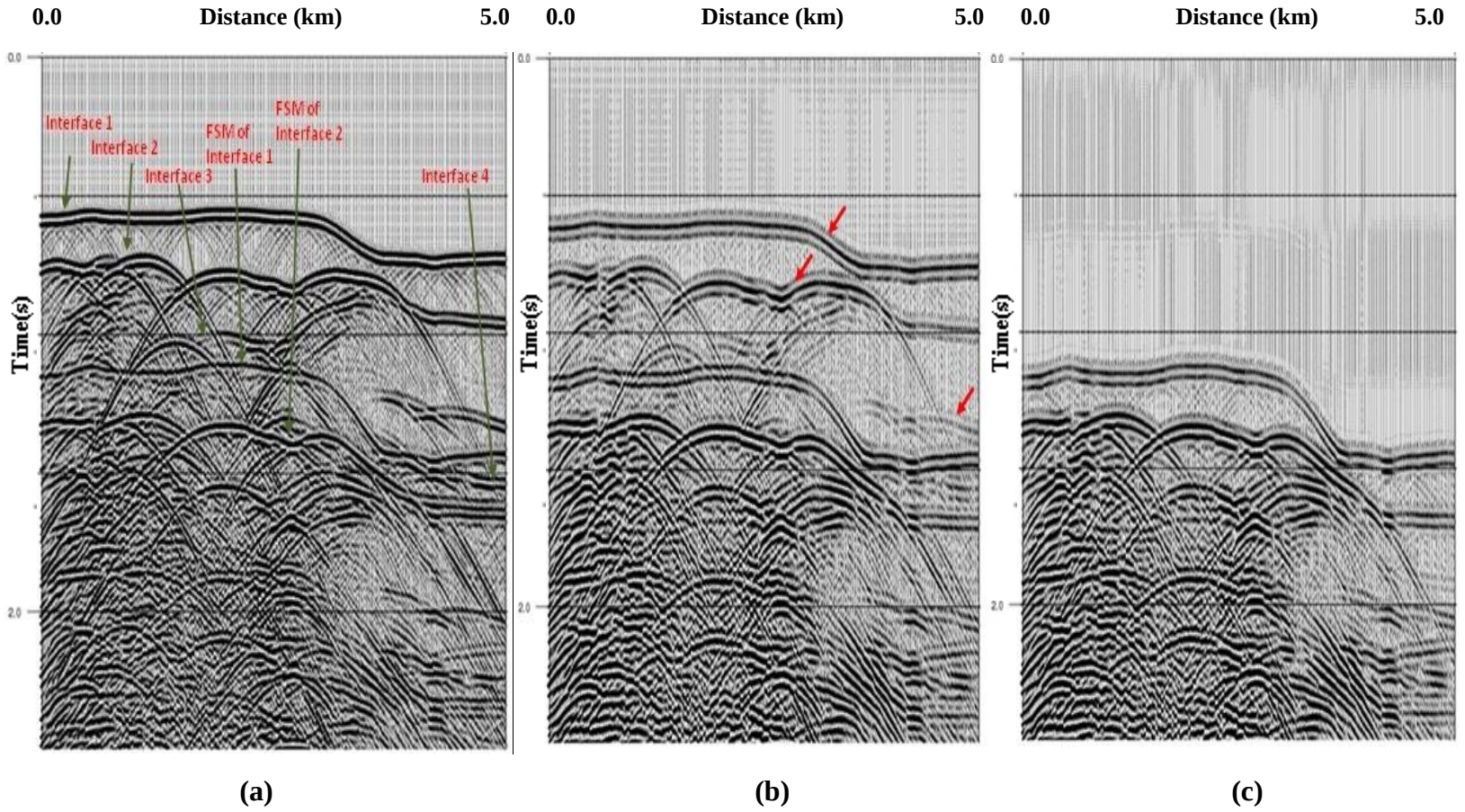

Figure 2.5. Illustration of the two predictions of the zero offset gather. (a) Illustration of the zero-offset gather of the synthetic data using the geology as illustrated in Figure 2.3a. (b) Illustration of the field P_1 after applying Equation (2.3). Notice that it contains receiver ghosts of primaries, free-surface multiples and receiver ghosts of free-surface multiples. The broad source signature here is due to the fact that P_1 involves the convolution between the two wavefields. (b) Illustration of the field P_1' after applying Equation (2.4). Notice that it does not contain the highlighted events in Figure 2.5b which are receiver ghosts of primaries. All the events contained in this figure are shown in Figure 2.5b which are free-surface multiples and their receiver ghosts.

Reconstruction of Receiver Ghosts of Primaries Using the Standard Subtraction Technique

In the previous section, we have described the two predictions based on the second term of the Kirchhoff scattering series. With the two predictions, we have generated two wavefields, P_1 and P_1'. In order to reconstruct receiver ghosts of primaries to image the subsurface from the two wavefields, we will provide one possible way in this section.

Let us start by taking the difference between P_1 and P_1'; i.e.,

$$P_{\mathrm{GP}}(\boldsymbol{x_s}, \boldsymbol{x_r}, t) = P_1(\boldsymbol{x_s}, \boldsymbol{x_r}, t) - \frac{3}{2} P_1'(\boldsymbol{x_s}, \boldsymbol{x_r}, t). \quad (2.5)$$

The factor $\frac{3}{2}$ here is due to the fact that P_1 predicts each first-order free-surface multiple once and the receiver ghost of each first-order free-surface multiple twice, whereas P_1' predicts the first-order free-surface multiple once but the receiver ghost of each first-order free-surface multiple only once. So equation (2.5) will essentially attenuate first-order free-surface multiples and receiver ghosts of first-order free-surface multiples. We applied equation (2.5) using the predictions in Figures 2.4 and 2.5. Figures 2.6 and 2.7 show the results of this subtraction in the form of a shot gather as well as an offset gather. Notice that a significant amount of energy has been removed through this subtraction, in particular first-order free-surface multiples and their receiver ghosts. However, almost all second- and higher-order free-surface multiples still remain in these data. That is why we will propose another algorithm in the next section.

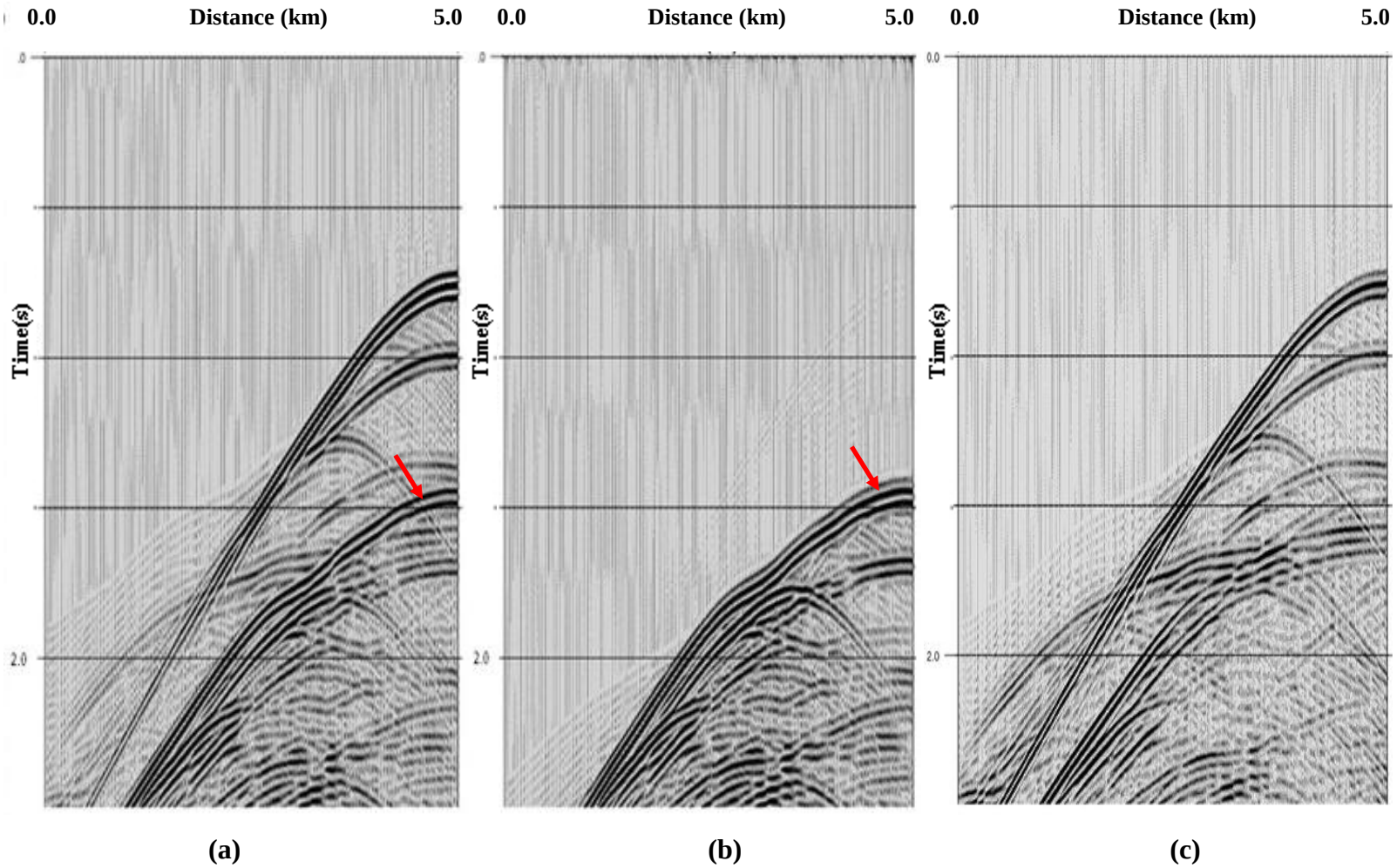

Figure 2.6. Illustration of standard subtraction results of the shot gather. (a) Illustration of the shot gather of the field P_1 after applying Equation (2.3). (b) Illustration of the shot gather of the field $P_1^{'}$ after applying Equation (2.4). (c) Illustration of the subtraction result between two wavefields P_1 and $P_1^{'}$ by using equation (2.6). Notice that the energy of the highlighted event which is first-order free-surface multiples is decreased a lot.

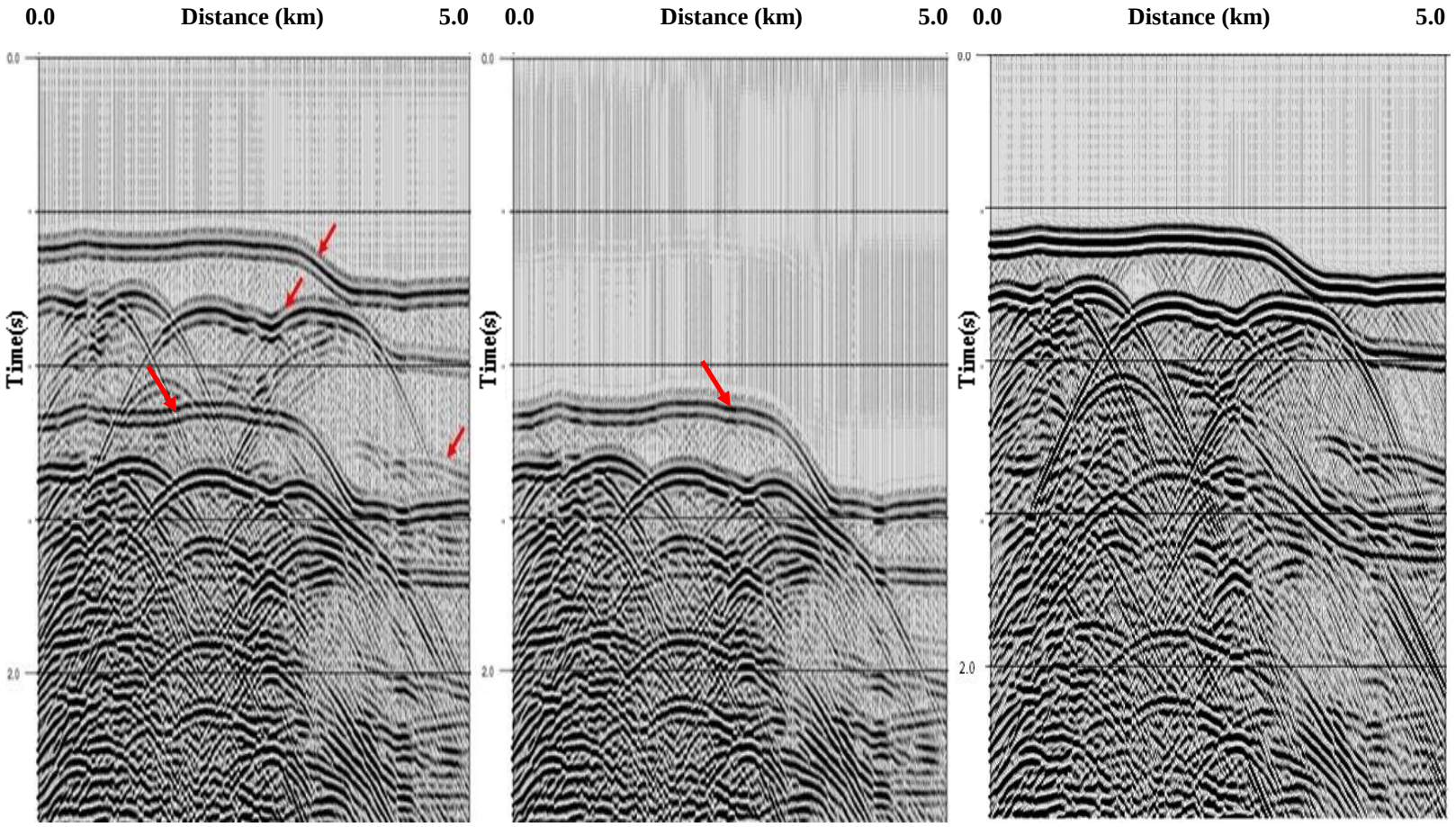

Figure 2.7. Illustration of standard subtraction results of the zero offset gather. (a) Illustration of the zero-offset gather of the field P_1 after applying Equation (2.3). (b) Illustration of the zero-offset gather of the field P_1' after applying Equation (2.4). (c) Illustration of the subtraction result between two wavefields P_1 and P_1' by using equation (2.6). Notice that the energy of the highlighted event which is first-order free-surface multiples is decreased a lot.

Note that equation (2.5) assumes that the two possible ways of predicting receiver ghosts of first-order free-surface multiples described in Figure 2.3 yield the same results. Our synthetic example here clearly shows that is the case. However, due to various acquisition uncertainties, equation (2.5) may sometimes not be applicable. In these cases, we suggest using the following formula:

$$P_{\mathrm{GP}}(\boldsymbol{x_s}, \boldsymbol{x_r}, t) = P_1(\boldsymbol{x_s}, \boldsymbol{x_r}, t) - a_{\mathrm{g}}(t)\, P_1'(\boldsymbol{x_s}, \boldsymbol{x_r}, t), \tag{2.6}$$

where a_{g} in this subtraction is designed to compensate for these uncertainties. The estimation of a_{g} is straightforward. By using derivations similar to those of Ikelle et al. (1997), we arrive at a stable, noniterative, and analytic solution (see Appendix B for more details), mainly because we have a linear relationship between the two unknowns in equation (2.6)—namely, the field P_{GP} and the scaling factor a_{g}.

Let us remark that the scaling function $\mathrm{a_g}$ is different from the inverse source signature, as required in the Kirchhoff scattering series in equation (2.1). Here $\mathrm{a_g}$ acts as a deghotsing operator, whereas a is a deconvolution operator. In fact, a is designed to compensate for the square of the source signature generated by the autoconvolution operation in the computation of P_1, for instance, so that the amplitudes of events with one bounce at the free surface in P_1 and P_0 can be comparable.

Reconstruction of Receiver Ghosts of Primaries Using a Combinatory Search

In the previous section, we described one possible way to recover the field of receiver ghosts of primaries. This method is based on the subtraction of two predicted wavefields P_1 and P_1', with a scaling factor a_g to adjust the amplitude of the first-order free-surface multiples in the two wavefields. However, if the data contain more than first-order free-surface multiples, the output of equation (2.5) includes receiver ghosts of primaries and second- and higher-order receiver ghosts of free-surface multiples, as illustrated in Figures 2.6 and 2.7.

In this section, we will propose a new way of reconstructing receiver ghosts of primaries. The basic idea of this approach is to pose the problem of reconstructing receiver ghosts of primaries as that of solving a system of two equations with three unknowns. The two predicted wavefields, P_1 and P_1', are used to construct the two equations. The three unknowns are (1) the receiver ghosts of primaries, (2) the free-surface multiples and their associated receiver ghosts in the wavefield containing receiver ghosts of primaries, and (3) the free-surface multiples and receiver ghosts of multiples contained in the other wavefield. These two equations can be described as follows:

$$P_1 = P_{\mathrm{RG}} + \mathrm{M} + 2\mathrm{M}_{\mathrm{RG}}^{(1)} + 3\mathrm{M}_{\mathrm{RG}}^{(2)} + 4\mathrm{M}_{\mathrm{RG}}^{(3)} + \ldots, \tag{2.7}$$

$$P_1' = \mathrm{M} + \mathrm{M}_{\mathrm{RG}}^{(1)} + 2\mathrm{M}_{\mathrm{RG}}^{(2)} + 3\mathrm{M}_{\mathrm{RG}}^{(3)} + \ldots, \tag{2.8}$$

where P_{RG} represents the receiver ghosts of primaries, M denotes the free-surface multiples, and $\mathrm{M}_{\mathrm{RG}}^{(\mathrm{i})}$ represents the receiver ghosts of the i^{th} order free-surface multiples (**i**

takes values $1, 2, 3, \ldots$). Notice the differences in the multiplicative factors between receiver ghosts of free-surface multiples predicted by P_1 and those predicted by P_1' in the two wavefields. Again, these differences are the reason why the subtraction scheme in equation (2.5) cannot be totally effective for all orders of multiples. Notice also that all the fields involved in equation (2.7) and (2.8) depend on source location $\boldsymbol{x_s}$, receiver location $\boldsymbol{x_r}$, and time t. We will often write these fields without these variables to keep the equation compact.

We have turned equation (2.7) and (2.8) into a system of two equations and three unknowns by rewriting them as follows:

$$Q_1 = P_{\mathrm{RG}} + \mathrm{M}', \tag{2.9}$$

$$Q_2 = P_1 - \frac{3}{2} P_1' = P_{\mathrm{RG}} + \mathrm{M}'', \tag{2.10}$$

where

$$\mathrm{M}' = \mathrm{M} + 2\mathrm{M}_{\mathrm{RG}}^{(1)} + 3\mathrm{M}_{\mathrm{RG}}^{(2)} + 4\mathrm{M}_{\mathrm{RG}}^{(3)} + \ldots, \tag{2.11}$$

$$\mathrm{M}'' = -\frac{1}{2}\mathrm{M} + \frac{1}{2}\mathrm{M}_{\mathrm{RG}}^{(1)} - \frac{1}{2}\mathrm{M}_{\mathrm{RG}}^{(3)} + \ldots. \tag{2.12}$$

Thus the two equations (2.9) and (2.10) can be written in the following form:

$$\begin{bmatrix} Q_1(\boldsymbol{x_s}, \boldsymbol{x_r}, t) \\ Q_2(\boldsymbol{x_s}, \boldsymbol{x_r}, t) \end{bmatrix} = \begin{bmatrix} 1 & 1 & 0 \\ 1 & 0 & 1 \end{bmatrix} \begin{bmatrix} P_{\mathrm{RG}}(\boldsymbol{x_s}, \boldsymbol{x_r}, t) \\ \mathrm{M}'(\boldsymbol{x_s}, \boldsymbol{x_r}, t) \\ \mathrm{M}''(\boldsymbol{x_s}, \boldsymbol{x_r}, t) \end{bmatrix}. \tag{2.13}$$

Here, we have explicitly added the variables to emphasize that these systems of equations hold for every given datapoint $(\boldsymbol{x_s}, \boldsymbol{x_r}, t)$. The system is underdetermined. So we propose to solve it by making additional assumptions. The assumption here is that for a given

datapoint, at least one of the three unknowns in equation (2.13) is zero. In other words, we solve the problem by solving the following set of three equations:

$$\begin{bmatrix} Q_1(\boldsymbol{x_s}, \boldsymbol{x_r}, t) \\ Q_2(\boldsymbol{x_s}, \boldsymbol{x_r}, t) \end{bmatrix} = \begin{bmatrix} 1 & 1 & 0 \\ 1 & 0 & 1 \end{bmatrix} \begin{bmatrix} P_{\mathrm{RG}}(\boldsymbol{x_s}, \boldsymbol{x_r}, t) \\ \mathrm{M}'(\boldsymbol{x_s}, \boldsymbol{x_r}, t) \\ 0 \end{bmatrix}, \tag{2.14}$$

$$\begin{bmatrix} Q_1(\boldsymbol{x_s}, \boldsymbol{x_r}, t) \\ Q_2(\boldsymbol{x_s}, \boldsymbol{x_r}, t) \end{bmatrix} = \begin{bmatrix} 1 & 1 & 0 \\ 1 & 0 & 1 \end{bmatrix} \begin{bmatrix} P_{\mathrm{RG}}(\boldsymbol{x_s}, \boldsymbol{x_r}, t) \\ 0 \\ \mathrm{M}''(\boldsymbol{x_s}, \boldsymbol{x_r}, t) \end{bmatrix}, \tag{2.15}$$

$$\begin{bmatrix} Q_1(\boldsymbol{x_s}, \boldsymbol{x_r}, t) \\ Q_2(\boldsymbol{x_s}, \boldsymbol{x_r}, t) \end{bmatrix} = \begin{bmatrix} 1 & 1 & 0 \\ 1 & 0 & 1 \end{bmatrix} \begin{bmatrix} 0 \\ \mathrm{M}'(\boldsymbol{x_s}, \boldsymbol{x_r}, t) \\ \mathrm{M}''(\boldsymbol{x_s}, \boldsymbol{x_r}, t) \end{bmatrix}. \tag{2.16}$$

For each datapoint, we select one of these solutions based on the assumption that the solution which has the smallest ℓ_1 norm is the correct one. More precisely, we are going to compute $F_1 = |P_{\mathrm{RG}}| + |\mathrm{M}'|$, $F_2 = |P_{\mathrm{RG}}| + |\mathrm{M}''|$, and $F_3 = |\mathrm{M}'| + |\mathrm{M}''|$. We will select the solution which corresponds to $\min(F_1, F_1, F_3)$.

The method we have just described for solving our underdetermined system is known as a combinatory search. Actually, the combinatory search is a minimization of the ℓ_0 norm. That is, we want to find the solution which has the maximum number of zero components.

Before we turn to the numerical result, let us just add a more mathematical definition of the ℓ_0 norm. Suppose that the left side of equation (2.13) is denoted as **Y**, the vector term on the right side is denoted as **X**, and the matrix is denoted by **A**. The combinatory search corresponding to finding **X** is as follows:

$$\min_{\mathbf{X}} \|\mathbf{X}\|_0 \quad subject\ to \quad \mathbf{Y} = \mathbf{AX}, \tag{2.17}$$

where

$$\|\mathbf{X}\|_0 = \sum_i |X_i|^0 = \#\{\mathbf{X}_i \neq 0\}. \tag{2.18}$$

The quantity $\|\mathbf{X}\|_0$ refers to the number of nonzero components of vector $\mathbf{X}$. That is the definition of the ℓ_0 norm.

The solution of the ℓ_0 norm minimization is known as sparse because it usually contains several zeros. Therefore, we are able to solve this 2×3 system here because of the sparsity assumption.

Let us recall that the ℓ_0 norm is just a particular case of well-known ℓ_p norms for the case where $p = 0$. The ℓ_p norms are defined as follows:

$$\|\mathbf{X}\|_P = \sum_i |X_i|^p \,, \tag{2.19}$$

or

$$\|\mathbf{X}\|_p^p = (\sum_i |X_i|^p)^{1/p}, \tag{2.20}$$

where $\|\,.\,\|_P$ denotes the ℓ_p norm. When $p = 2$, it becomes the classical ℓ_2 norm. When $p = 0$, it is the ℓ_0 norm which measures the number of nonzero components in vector $\mathbf{X}$.

Before we turn to a discussion of the results of the approach that we have just outlined, let us first analyze all the events in wavefield P_1. We have noted that field P_1 contains receiver ghosts of primaries, free-surface multiples, and receiver ghosts of free-surface multiples. Figure 2.8a illustrates our interpretation of wavefield P_1. The red lines represent the receiver ghosts of primaries, whereas the yellow lines represent the free-

surface multiples and their receiver ghosts. M_1 is the first free-surface multiple in this shot gather. Thus all the events before M_1 are receiver ghosts of primaries. We have identified all the other multiples in this figure—for example, M_2 and M_3. After a detailed analysis of this shot gather, we observe that all the events located below M_3 are multiples.

Let us now turn to an analysis of the effectiveness of our demultiple process based on a combinatory search. We will compare the results of the combinatory search based on demultiple to those based on subtraction schemes in the previous section. Figure 2.8 shows side by side the result of the subtraction-based demultiple and the result based on the combinatory search. We can see that both of these results preserve the receiver ghosts of primaries. Moreover, the two methods are effective in attenuating all multiple events located above M_3. However, we can notice that the subtraction-based demultiple is not effective for removing events below M_3 because these events are mostly second-order multiples. As we discussed in the previous section, the subtraction based-demultiple is effective only for one-order multiples. In this thesis, we use it to attenuate first-order multiples only. By contrast, we can see that the combinatory-search-based demultiple result shown in Figure 2.8c is effective even for removing events below M_3. In other words, the combinatory-search-based demultiple method allows us to attenuate several-order multiples simultaneously. All the observations above also hold for offset gather data, as illustrated in Figure 2.9.

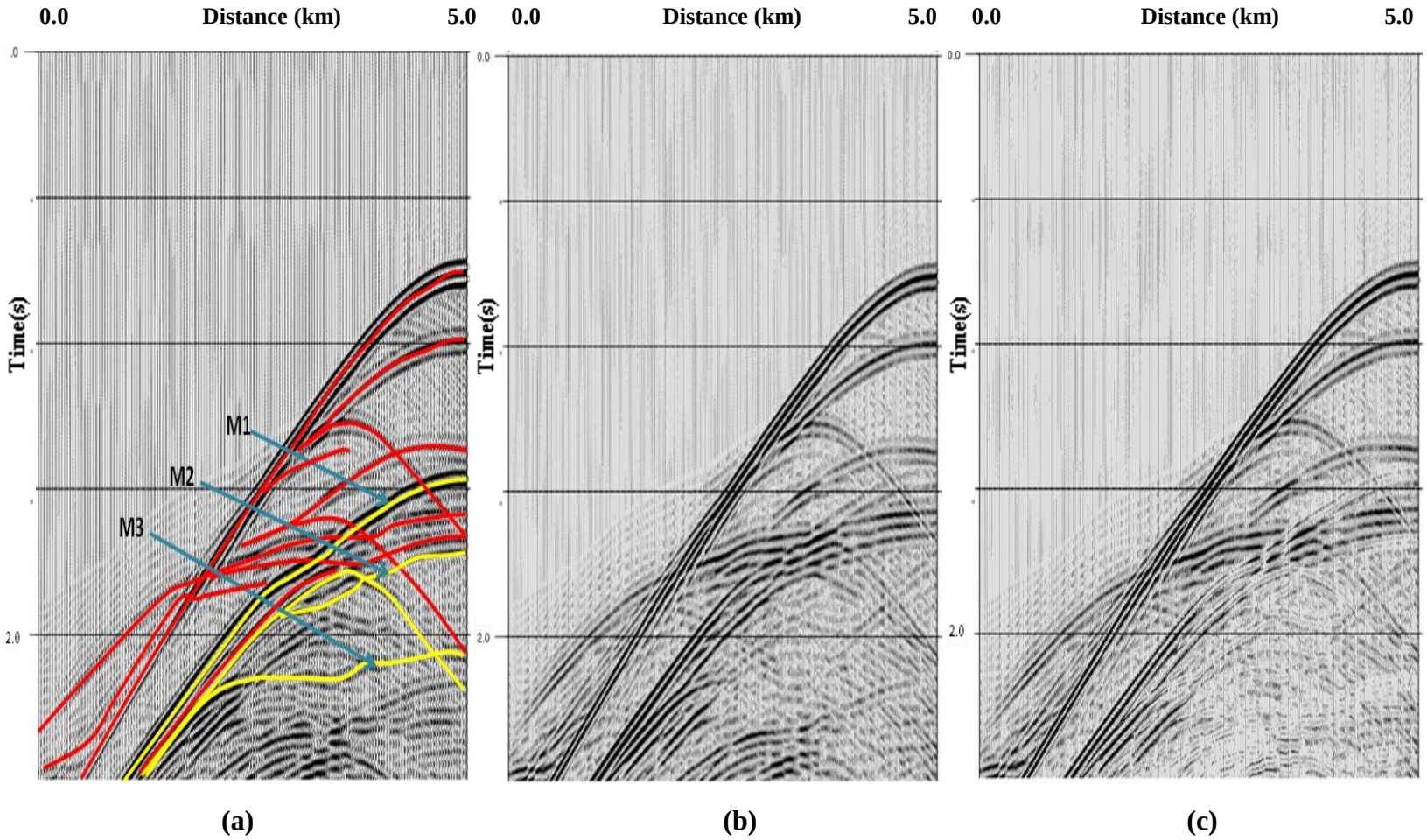

Figure 2.8. Illustration of combinatory search based demultiple results of the shot gather. (a) Illustration of the shot gather of the field P_1 after applying Equation (2.3). (b) Illustration of the standard subtraction result after applying Equation (2.6). (c) Illustration of the solution of equation (2.14) to (2.16) by using combinatory search. Notice that the highlighted events in red color are receiver ghosts of primaries and the highlighted events in yellow color are free-surface multiples. M_1, M_2 and M_3 denotes the three free-surface multiples highlighted.

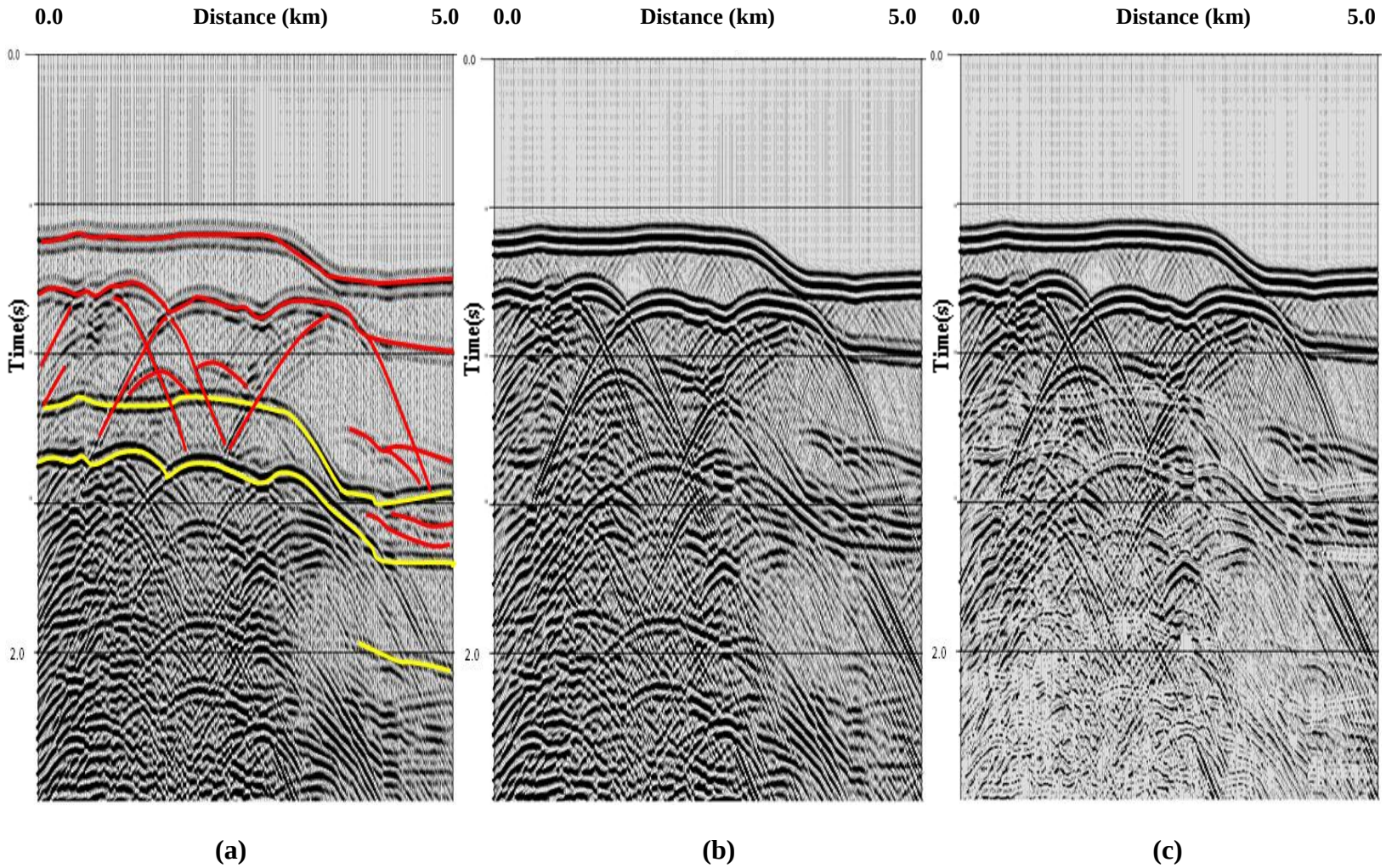

Figure 2.9. Illustration of combinatory search based demultiple results of the zero offset gather. (a) Illustration of the zero-offset gather of the field P_1 after applying Equation (2.3). (b) Illustration of the standard subtraction result after applying Equation (2.6). (c) Illustration of the solution of equation (2.14) to (2.16) by using combinatory search. Notice that the highlighted events in red color are receiver ghosts of primaries and the highlighted events in yellow color are free-surface multiples.

CHAPTER III

SUMMARY: ADVANTAGES OF RECONSTRUCTING RECEIVER GHOSTS OF PRIMARIES INSTEAD OF PRIMARIES THEMSELVES

In Chapter II, we described our multiple-attenuation schemes for reconstructing receiver ghosts of primaries. By taking advantage of the sparsity of the seismic data, we can reconstruct the field of receiver ghosts of primaries from the two predictions [equations (2.3) and (2.4)], which are based on the second term of the Kirchhoff scattering series.

In this chapter, we will focus on discussions of the advantages of our approach in Chapter II in contrast to the Kirchhoff multiple-attenuation scheme described in Chapter I. We will start by discussing the savings in computer storage and computation time of the new approach.

In Chapter I, we discussed the two important drawbacks which limited the application of the Kirchhoff scattering series. One is the requirement of acquiring very large 3D datasets that are beyond the capability of current seismic-acquisition technology. The other is the requirement of acquiring near-offset (including zero-offset) data. Our new approach in Chapter II might overcome the first drawback, and we will discuss this possibility in the second section.

Savings Associated with the New Implementation of the Kirchhoff Series Multiple Attenuation Scheme

Let us consider a typical seismic exploration case in which the data length is 6 seconds, the water depth is 250 m, and the sea-bottom reflection is 0.3 at normal incidence. The demultiple process requires the removal of more than first-order free-surface multiples in this case. Actually, our experience suggests that we will need to compute at least the first four orders of multiples to remove all free-surface multiples from the data.

If we use the Kirchhoff scattering series in equations (2.1) and (2.2) to remove these multiples, we have to compute P_1, P_2, P_3, and P_4. The computation of P_2 requires the field P_1, the computation of P_3 requires the field P_2, and so on. So the iteration in equation (2.2) does not allow us to compute all of them in parallel.

If we use our demultiple scheme based on the second term of the Kirchhoff scattering series and combinatory search, we need only to compute P_1 and P_1'. The computation of P_1 and P_1' can be carried out in parallel. Thus we eliminate the computation of P_2, P_3, and P_4 and their storage requirements.

Based on the discussion above, the savings in data storage and computation time relative to the new implementation of the Kirchhoff scattering series multiple-attenuation scheme described in equation (2.3)-(2.4) can be significant if the demultiple process requires the removal of more than first-order free-surface multiples. The elimination of the computation of the higher-order terms of the new implementation of the Kirchhoff

scattering series multiple-attenuation scheme in this thesis produces at least a fourfold savings in data storage and computation time in this case.

A Potential Way of Avoiding Surface Integrals

Equations (2.3) and (2.4) give us the computation of P_1 and P_1' in compact form. To illuminate our point in this section, we rewrite these two equations in the following form:

$$P_1(x_r, y_r, \omega, x_s, y_s) = \int_{-\infty}^{+\infty} dx \int_{-\infty}^{+\infty} dy\, P_0(x_r, y_r, \omega, x, y) \times v_z(x, y, \omega, x_s, y_s), \quad (3.1)$$

$$P_1'(x_r, y_r, \omega, x_s, y_s) = \int_{-\infty}^{+\infty} dx \int_{-\infty}^{+\infty} dy\ P_0^{(nd)}(x_r, y_r, \omega, x, y) \times v_z(x, y, \omega, x_s, y_s). \quad (3.2)$$

Note that this equation requires a surface integral over x and y in infinite space. Thus we need to acquire a very large 3D dataset with well-distributed sources and receivers along the x and y directions to correctly perform these integrals. However, the current seismic-acquisition technology cannot obtain such datasets, as we have discussed in Chapter I.

In our new implementation of the Kirchhoff scattering series multiple-attenuation scheme described in equations (2.3) and (2.4), because we are actually concerned here with the differences between P_1 and P_1', we propose to compute P_1 and P_1' with line integrals as follows:

$$\tilde{P}_1(x_r, y_r, \omega, x_s, y_s) = \int_{-\infty}^{+\infty} dx\, P_0(x_r, y_r, \omega, x, y_s) \times v_z(x, y_s, \omega, x_s, y_s), \quad (3.3)$$

$$\tilde{P}_1'(x_r, y_r, \omega, x_s, y_s) = \int_{-\infty}^{+\infty} dx\, P_0^{(nd)}(x_r, y_r, \omega, x, y_s) \times v_z(x, y_s, \omega, x_s, y_s). \quad (3.4)$$

Most 3D errors in $\tilde{P}_1$ and $\tilde{P}_1'$ are similar. Therefore, the subtraction of $\tilde{P}_1$ and $\tilde{P}_1'$ is likely to be unaffected by 3D errors. Figure 2.3 actually illustrates one scenario in which the subtraction may turn out to be effective. The receiver ghosts of multiples can be constructed as a multidimensional convolution of a multiple with a direct wave, or as a multiple (primary) with a receiver ghost of a multiple (a receiver ghost of a primary). If the scattering points at the sea surface between these two constructions are different, then the subtraction may be ineffective.

To overcome the potential residual that may be left after taking the difference between$\tilde{P}_1$ and $\tilde{P}_1'$, we suggest performing a second combinatory search that involves the actual data P_0. If we denote $\mathrm{d}\tilde{P}_1$ as the result of our subtractions, then we can pose the problem of recovering the primaries as follows:

$$P_0 = \mathcal{P}p + \mathrm{M}, \tag{3.5}$$

$$a\,\mathrm{d}\tilde{P}_1 = \mathcal{P}p + \mathrm{R}, \tag{3.6}$$

where M represents multiples in the data, R is the residual left after subtraction, and a is the source signature.

REFERENCES

Aki, K., and Richards, P. G., 1980, Quantitative seismology: W. H. Freeman and Co.

Amundsen, L., 2001, Elimination of free-surface related multiples without need of the source wavelet: Geophysics **66**, 327-341.

Amundsen, L., Ikelle, L. T., and Berg, L. E., 2001, Multidimensional signature deconvolution and free-surface multiple elimination of 4C data: Geophysics, **66**, 1594-1604.

Gangi, A. F., 1970, A derivation of the seismic representation theorem using seismic reciprocity: J. Geophys. Res., **75**, 2088-2095.

Ikelle, L. T., and Jaeger, R., 1997, A sensitivity analysis of inverse scattering multiple attenuation to shallow water: J. Seis. Expl., **8**, 331-350.

Ikelle, L. T., Roberts, G., and Weglein, A.B., 1997, Source signature estimation based on the removal of first-order multiples: Geophysics, **62**, 1904-1920.

Ikelle, L. T., Amundsen, L., Gangi, A. F. and Wyatt, S., 2003, Kirchhoff scattering series. Insight into the multiple attenuation method: Geophysics **68**, 16-28.

Ikelle, L. T. and Amundsen L., 2005, An introduction to petroleum seismology: Society of Exploration Geophysics.

Osen, A., Amundsen, L., and Reitan, R., 1999, Removal of water-layer multiples from multicomponent sea-bottom data: Geophysics, **64**, 835-851.

Sommerfield, A., 1954, Optics: Academic Press.

Verrchuur, D. J., Berkhout, A. J., and Wapenaar, C. P. A., 1992, Adaptive Surface-related multiple elimination: Geophysics, **57**, 1166-1177.

Watts, A., and Ikelle, L. T., 2006, Linear demultiple solution based on the concept of bottom multiple generator (BMG) approximation: some new results: Geophysical Prospective, **54**, 492-497.

APPENDIX A

FINITE DIFFERENCE MODELING

Finite difference modeling (FDM) is one of the most accurate numerical techniques for solving the differential equations which describe wave propagation in the earth, under a set of initial, final, and boundary conditions. In this research, we used FDM technique to generate the synthetic data. The two basic approaches to implementing FDM for the simulation of seismic surveys are the explicit approach and the implicit approach. We will focus on explicit approach which wave equations are expressed in the time domain and are solved recursively, time step by time step. We will follow Appendix C of Ikelle and Amundsen (2005) to describe explicit approach.

Basic Equations for Elastodynamic Wave Motion in Elastic Media

The governing equations for the wave propagation are as follows:

1) The equations of momentum conservation are

$$\rho(\boldsymbol{x})\partial_t v_x(\boldsymbol{x},t) - \{\partial_x \tau_{xx}(\boldsymbol{x},t) + \partial_z \tau_{xz}(\boldsymbol{x},t)\} = f_x(\boldsymbol{x},t), \quad (1)$$

$$\rho(\boldsymbol{x})\partial_t v_z(\boldsymbol{x},t) - \{\partial_x \tau_{xz}(\boldsymbol{x},t) + \partial_z \tau_{zz}(\boldsymbol{x},t)\} = f_z(\boldsymbol{x},t), \quad (2)$$

where the components of the particle velocity are denoted as $\boldsymbol{v} = (v_x, v_z)$, $\boldsymbol{\tau} = (\tau_{xx}, \tau_{yy}, \tau_{xz})$ are the stress components, and $\boldsymbol{f} = (f_x, f_z)$ are the components of the body force.

2) The stress-strain relationships for an isotropic elastic medium are as follows:

$$\partial_t \tau_{xx}(\boldsymbol{x},t) = [\lambda(\boldsymbol{x}) + 2\mu(\boldsymbol{x})]\partial_x v_x(\boldsymbol{x},t) + \lambda(\boldsymbol{x})\partial_z v_z(\boldsymbol{x},t) + I_{xx}(\boldsymbol{x},t), \quad (3)$$

$$\partial_t \tau_{zz}(\boldsymbol{x},t) = [\lambda(\boldsymbol{x}) + 2\mu(\boldsymbol{x})]\partial_z v_z(\boldsymbol{x},t) + \lambda(\boldsymbol{x})\partial_x v_x(\boldsymbol{x},t) + I_{zz}(\boldsymbol{x},t), \quad (4)$$

$$\partial_t \tau_{xx}(\boldsymbol{x},t) = \mu(\boldsymbol{x})[\partial_z v_x(\boldsymbol{x},t) + \partial_x v_z(\boldsymbol{x},t)] + I_{xz}(\boldsymbol{x},t). \quad (5)$$

In these equations, $\boldsymbol{I} = (I_{xx}, I_{yy}, I_{xz})$ are the components of the stress-rate source, so the wave motion satisfies a set of first-order coupled differential equations (1) through (5).

To solve equations (1) through (5), it is essential to specify the appropriate boundary and initial conditions for the problem of modeling wave propagation through the subsurface. The initial conditions are that the stress and particle-velocity fields and their time derivatives are null before the seismic source is fired; that is:

$$\boldsymbol{v} = \partial_t \boldsymbol{v} = \boldsymbol{0}, \ t \leq 0,$$

$$\boldsymbol{\tau} = \partial_t \boldsymbol{\tau} = \boldsymbol{0}, \quad t \leq 0. \quad (6)$$

The boundary conditions for the problem of modeling seismic wave propagation are determined by the free-surface boundary: air-solid in the case of land seismic and air-water in the case of marine seismic. Let us assume the free surface to be at a depth level of $z = 0$. Then, the boundary conditions are:

$$\tau_{zz}(x, z = 0, t) = \tau_{xz}(x, z = 0, t) = 0, \quad (7)$$

or, equivalently,

$$[\lambda(\boldsymbol{x}) + 2\mu(\boldsymbol{x})]\partial_z v_z(x, z = 0, t) + \lambda(\boldsymbol{x})\partial_x v_x(x, z = 0, t)$$
$$= \mu(\boldsymbol{x})[\partial_z v_x(x, z = 0, t) + \partial_x v_z(x, z = 0, t)] = 0. \quad (8)$$

We consider the rest of the medium to be unbounded.

Discretization in Both Time and Space

The first step in finite difference modeling is to describe the geologic model and the quantities that characterize the wavefield, that is, the particle velocity and stresses, in this case. We discretize both the time and space domains as follows:

$$t = n\Delta t, \qquad n = 0,1,2,\dots,N,$$

$$x = i\Delta x, \qquad i = 0,1,2,\dots,I,$$

$$z = k\Delta x, \qquad k = 0,1,2,\dots,K. \tag{9}$$

This discritezation is called the reference grid.

In standard finite-difference calculations, each quantity in the differential equations (1) through (5) can now be defined as a function of the indexes n, i, and k, in accordance with the following two examples:

$$\lambda(x,z) = \lambda\left[\left(i+\frac{1}{2}\right)\Delta x, \left(k+\frac{1}{2}\right)\Delta x\right] = \lambda_{\mathrm{i+1/2,k+1/2}}$$

$$\tau_{xz}(x,z,t) = \tau_{xz}(i\Delta x, k\Delta x, n\Delta t) = [\tau_{xz}]_{i,k}^{n}. \tag{10}$$

In the staggered-grid technique, not all quantities in the differential equations (1) through (5) are gridded at the points of the reference grid. Some quantities are defined as being half a grid point off the reference grid, say, $i = \left(i \pm \frac{1}{2}\right)\Delta x$, instead of $x = i\Delta x$. Figure 1 shows an example of staggered gridding of the quantities entering in the equations (1) through (5). Note that the shear stresses are defined at the points on the reference grid, whereas the normal stresses, the three components of the particle velocity, the mass density, and the Lamė parameters, are defined as the points half a grid off the

reference grid. Notice also that normal stresses, mass density, and the Lamė parameters, are located at the same points.

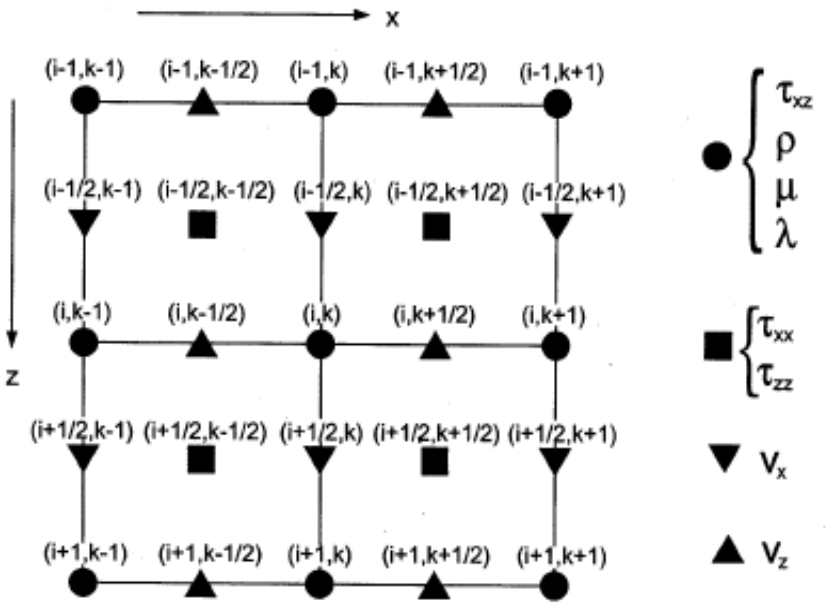

Figure A.1. Illustration of the staggered grid for 2D elastic finite-difference modeling (Ikelle and Amundsen,2003).

Staggered Grid Implementation

The discrete forms of equations (1) through (5) are given by Madariaga (1976) and Graves (1996) as

$$[v_x]_{i,k+1/2}^{n+1/2} = [v_x]_{i,k+1/2}^{n-1/2} + [\Delta\, tb_x(D_x\tau_{xx} + D_z\tau_{xz} + f_x)]_{i,k+1/2}^{n}, \quad (11)$$

$$[v_z]_{i+1/2,k}^{n+1/2} = [v_z]_{i+1/2,k}^{n-1/2} + [\Delta\, tb_z(D_x\tau_{xz} + D_z\tau_{zz} + f_z)]_{i+1/2,k}^{n}, \quad (12)$$

for particle velocity, and

$$[\tau_{xx}]_{\mathrm{i}+1/2,\mathrm{k}+1/2}^{n+1} = [\tau_{xx}]_{\mathrm{i}+1/2,\mathrm{k}+1/2}^{n} + \Delta\, t[(\lambda + 2\mu)D_x v_x + \lambda D_z v_z + I_{xx}]_{\mathrm{i}+1/2,\mathrm{k}+1/2}^{n+1/2}, \quad (13)$$

$$[\tau_{zz}]_{\mathrm{i}+1/2,\mathrm{k}+1/2}^{n+1} = [\tau_{zz}]_{\mathrm{i}+1/2,\mathrm{k}+1/2}^{n} + \Delta\, t[(\lambda + 2\mu)D_z v_z + \lambda D_x v_x + I_{zz}]_{\mathrm{i}+1/2,\mathrm{k}+1/2}^{n+1/2}, \quad (14)$$

$$[\tau_{xz}]_{i,k}^{n+1} = [\tau_{xz}]_{i,k}^{n} + \Delta\, t[\mu_{xz}(D_z v_x + D_x v_z) + I_{xz}]_{i,k}^{n+1/2}, \quad (15)$$

for the stresses, with

$$b_x = \frac{1}{2}\left[b_{i,k} + b_{i-1,k}\right], \quad (16)$$

$$b_z = \frac{1}{2}\left[b_{i,k} + b_{i,k-1}\right], \quad (17)$$

$$\mu_{xz} = \left[\frac{1}{4}\left(\frac{1}{\mu_{i,k}} + \frac{1}{\mu_{i-1,k}} + \frac{1}{\mu_{i,k-1}} + \frac{1}{\mu_{i-1,k-1}}\right)\right]^{-1}. \quad (18)$$

In these equations, b_x and b_z are the effective-medium parameters for the reciprocal of density, and μ_{xz} is the effective-medium parameter for the rigidity. The operators, D_x and D_z denote the first-order spatial derivative for x and z, respectively. Note that the first-order spatial-derivative operators are generally evaluated by either a second-order

difference or a fourth-order difference. For this research we use the fourth-order difference that is,

$$D_x g_{i,k} \approx \frac{1}{\Delta x}\left[\frac{9}{8}\left(g_{\mathrm{i}+1/2,\mathrm{k}} - g_{\mathrm{i}-1/2,\mathrm{k}}\right) - \frac{1}{24}\left(g_{\mathrm{i}+3/2,\mathrm{k}} - g_{\mathrm{i}-3/2,\mathrm{k}}\right)\right]. \quad (19)$$

The forth-order finite-difference approximation requires a minimum sampling of five grid points per wavelength (Levander, 1988).

Stability Condition

In the staggered-grid finite-difference equations (11) through (15), the five quantities $\{v_x, v_z, \tau_{xx}, \tau_{zz}, \tau_{xz}\}$ characterizing the wave motion are computed recursively, time step by time step. However, this recursive computation (time step by time step) can be the source of numerical instability. In fact, errors introduced by the numerical solution can propagate and be magnified during time-stepping of the finite-difference scheme, thereby causing significant instabilities during the computation and artifacts in the resulting data. Such instability is very unlikely to occur if the ratio between the temporal and spatial sampling intervals is constrained as follows:

$$\Delta t < 0.606\frac{\Delta x}{v_{max}}, \quad (20)$$

where v_{max} is the maximum wave speed in the 2D model under consideration (Levander, 1988). Condition (20) is necessary, but it is not sufficient, because it is derived for homogeneous media; the derivation of stability for heterogeneous media generally is quite complicated.

Grid Dispersion

Approximation of spatial derivatives creates the grid dispersion. The condition for avoiding grid dispersion is related to the number of grid points per wavelength. In this research, we use the fourth-order approximation in equation (20) which requires a minimum sampling of five grid points per wavelength (Levander, 1988).

Boundary Condition

The free-surface boundary condition given in equation (7) is that the normal stress,τ_{zz}, and the shear stress, τ_{xz}, are null at $z = 0$. The horizontal spatial derivative poses no problem for staggered-grid implementation in equations (11) through (15). However, for the vertical spatial derivative, we have to add the two grid points above $z = 0$. If we assume antisymmetry for the stress components at $z = 0$, then the fields at and above the free surface are given as

$$[\tau_{xz}]_{i,k=0}^{n+1} = 0, [\tau_{xz}]_{i,k=-1}^{n+1} = -[\tau_{xz}]_{i,k=1}^{n+1} \quad (21)$$

and

$$[\tau_{zz}]^{n+1}_{i+1/2,k=-1/2} = -[\tau_{zz}]^{n+1}_{i+1/2,k=1/2}\,, \tag{22}$$

$$[\tau_{zz}]^{n+1}_{i+1/2,k=-3/2} = -[\tau_{zz}]^{n+1}_{i+1/2,k=3/2}\,. \tag{23}$$

Notice that the free-surface boundary conditions also can be addressed by literally adding an air-filled layer as the first layer of the geologic model. In the marine case, for instance, the water layer will be overlain by this air-filled layer.

We will consider the rest of the medium to be unbounded; in other words, we treat the other boundaries as having an absorbing boundary. The stress and particle-velocity fields are multiplied by the factor

$$G(i) = \exp\left\{-\left[\frac{\alpha}{iabmax}(iabmax - i)\right]^2\right\} \qquad for\ 1 \le i \le iabmax, \tag{24}$$

where $iabmax$ is the strip width in grid points and α is a constant determined, by trial and error, for the optimal absorbing boundary conditions.

APPENDIX B

ESTIMATION OF SCALING FUNCTION FOR THE REMOVAL OF FIRST-ORDER MULTIPLES

Ikelle et al. (2003) showed that the Kirchhoff scattering series for removing events caused by free-surface reflections (i.e., free-surface multiples) from seismic data $P_0(\mathrm{k}_s, \mathrm{k}_g, \omega)$ can be written as:

$$\mathcal{P}p(k_s, k_g, \omega) = P_0(k_s, k_g, \omega) - A(\omega)P_1(k_s, k_g, \omega) + A^2(\omega)P_2(k_s, k_g, \omega) - \ldots, \quad (1)$$

where $\mathcal{P}p(\mathrm{k}_s, \mathrm{k}_g, \omega)$ is the data without free-surface multiples and $A(\omega)$ is the inverse source signature. The field $P_1(\mathrm{k}_s, \mathrm{k}_g, \omega)$, $P_2(\mathrm{k}_s, \mathrm{k}_g, \omega)$, etc., are given by:

$$P_n(\mathrm{k}_s, \mathrm{k}_g, \omega) = \int_{-\infty}^{+\infty} dk\, P_{n-1}(\mathrm{k}_s, \mathrm{k}, \omega) \times v_z(\mathrm{k}, \mathrm{k}_g, \omega). \quad (2)$$

Notice that we use the data in (ω, k) domain. The Fourier-transformed variables corresponding to $\mathrm{x}_s, \mathrm{x}_g$, and t are, respectively, $\mathrm{k}_s, \mathrm{k}_g$ and ω.

For the application of the standard subtraction based on second term of Kirchhoff scattering series described in Chapter II, we need require the scaling factor $a_g(\omega)$, which is compensate for removing first-order multiples. Ikelle et al. (1997) gives a possible solution for this problem and we will follow those of this paper to solve our problem in this section.

The removal of the first order multiples corresponds to the truncation of the scattering series in Equation (1) to its first two terms. Equation (1) becomes:

$$\tilde{\mathcal{P}}p(\mathrm{k}_s, \mathrm{k}_g, \omega) = P_0(\mathrm{k}_s, \mathrm{k}_g, \omega) - A(\omega)P_1(\mathrm{k}_s, \mathrm{k}_g, \omega), \quad (3)$$

where $\tilde{\mathcal{P}}p(\mathrm{k}_s, \mathrm{k}_g, \omega)$ is the data without first-order multiples.

To take into account the truncation effects, we modify equation (3) to:

$$\tilde{\mathcal{P}}p(\mathrm{k}_s, \mathrm{k}_g, \omega) = P_0(\mathrm{k}_s, \mathrm{k}_g, \omega) - A(\omega)P_1(\mathrm{k}_s, \mathrm{k}_g, \omega) + \epsilon_{\mathrm{T}}, \quad (4)$$

where ϵ_{T} describes the effects caused by truncation. We suppose that ϵ_{T} is mall and nonlinear related to the inverse source $A(\omega)$.

We now introduce the minimum-energy criterion in the context of inverse problem theory. We use the least square norm. The "best source" in the least-squares sense is defined as $A(\omega)$ that minimizes to:

$$S(A) = \left\|\tilde{\mathcal{P}}p\right\|^2 + \|\mathrm{A}\|^2, \quad (5)$$

where

$$\left\|\tilde{\mathcal{P}}p\right\|^2 = \int \mathrm{d}k_g \int \mathrm{d}k_s \int \mathrm{d}\omega\, \tilde{\mathcal{P}}p(\mathrm{k}_s, \mathrm{k}_g, \omega) \times W_{\mathrm{D}}(\mathrm{k}_s, \mathrm{k}_g, \omega)\tilde{\mathcal{P}}p^*(\mathrm{k}_s, \mathrm{k}_g, \omega), \quad (6)$$

and

$$\|\mathrm{A}\|^2 = \sigma^2 \int d\omega \int d\omega' A(\omega)W_A^{-1}(\omega, \omega')\mathrm{A}^*(\omega'). \quad (7)$$

The asterisk denotes a complex conjugate. The weighting function $W_{\mathrm{D}}(\mathrm{k}_s, \mathrm{k}_g, \omega)$ describes errors in the data, and $W_A(\omega, \omega')$ describes the a priori information on the source. The term $\|\mathrm{A}\|^2$ is introduced to guarantee the stability of the solution. To simplify subsequent inversion formulas, we also have introduced the constant σ^2 in the definition of $\|\mathrm{A}\|^2$.

If we neglect truncation errors in the forward problem (equation (4)), the minimization problem in equation (5) gives the analytical solution

$$A_\omega^{(0)} = \frac{-\int d\omega' W_A(\omega,\omega')\mathrm{N}(\omega')}{\sigma^2 + \int d\omega' W_A(\omega,\omega')\mathrm{Q}(\omega')}, \quad (8)$$

where

$$\mathrm{N}(\omega') = \int \mathrm{d}k_g \int \mathrm{d}k_s \, P_0(\mathrm{k}_s, \mathrm{k}_g, \omega) \times W_\mathrm{D}(\mathrm{k}_s, \mathrm{k}_g, \omega) {P_1}^*(\mathrm{k}_s, \mathrm{k}_g, \omega), \tag{9}$$

and

$$\mathrm{Q}(\omega') = \int \mathrm{d}k_g \int \mathrm{d}k_s \, P_1(\mathrm{k}_s, \mathrm{k}_g, \omega) \times W_\mathrm{D}(\mathrm{k}_s, \mathrm{k}_g, \omega) {P_1}^*(\mathrm{k}_s, \mathrm{k}_g, \omega). \tag{10}$$

To accommodate truncation errors, we set up an iterative scheme, where $A_\omega^{(0)}$ is the starting solution. The initialization step consists of

$$\tilde{\mathcal{P}} p^{(0)}(\mathrm{k}_s, \mathrm{k}_g, \omega) = P_0(\mathrm{k}_s, \mathrm{k}_g, \omega) - A_\omega^{(0)} P_1(\mathrm{k}_s, \mathrm{k}_g, \omega), \tag{11}$$

and

$${P_0}^{(1)}(\mathrm{k}_s, \mathrm{k}_g, \omega) = \tilde{\mathcal{P}} p^{(0)}(\mathrm{k}_s, \mathrm{k}_g, \omega). \tag{12}$$

In general, $A_\omega^{(0)}$ permits a significant reduction of first-order multiple energy through $\tilde{\mathcal{P}} p^{(0)}(\mathrm{k}_s, \mathrm{k}_g, \omega)$. The iterations can be described as follows. For a given ${P_0}^{(\mathrm{n})}(\mathrm{k}_s, \mathrm{k}_g, \omega)$, a data set containing the residual energy of first-order multiples, we first compute ${P_1}^{(\mathrm{n})}(\mathrm{k}_s, \mathrm{k}_g, \omega)$ using equation (2). Second, we seek a correction $\delta A^{(n)}(\omega)$ to $A^{(n)}(\omega)$ by minimizing

$$S(\delta A^{(n)}) = \left\| \tilde{\mathcal{P}} p^{(\mathrm{n})} \right\|^2 + \left\| \mathrm{A}^{(\mathrm{n})} \right\|^2. \tag{13}$$

The solution of this minimization, denoted here as $\delta A^{(n)}(\omega)$, is similar to that described in equation (8). We only have to replace $P_0(\mathrm{k}_s, \mathrm{k}_g, \omega)$ with ${P_0}^{(\mathrm{n})}(\mathrm{k}_s, \mathrm{k}_g, \omega)$ and $P_1(\mathrm{k}_s, \mathrm{k}_g, \omega)$ with ${P_1}^{(\mathrm{n})}(\mathrm{k}_s, \mathrm{k}_g, \omega)$. We finish each iteration by updating the source as:

$$A^{(n)}(\omega) = A^{(n-1)}(\omega) + \delta A^{(n)}(\omega) \tag{14}$$

and the data as

$$\tilde{\mathcal{P}}p^{(\mathrm{n})}\left(\mathrm{k}_s, \mathrm{k}_g, \omega\right) = P_0{}^{(\mathrm{n})}\left(\mathrm{k}_s, \mathrm{k}_g, \omega\right) - \delta A^{(n)}(\omega)\, P_1{}^{(\mathrm{n})}\left(\mathrm{k}_s, \mathrm{k}_g, \omega\right), \tag{15}$$

and

$$P_0{}^{(\mathrm{n}+1)}\left(\mathrm{k}_s, \mathrm{k}_g, \omega\right) = \tilde{\mathcal{P}}p^{(\mathrm{n})}\left(\mathrm{k}_s, \mathrm{k}_g, \omega\right). \tag{16}$$

The iterations are stopped when two successive solutions $A^{(n)}(\omega)$ and $A^{(n-1)}(\omega)$ are close enough.

VITA

Name: Nan Ma

Address: Seismic Processing, ConocoPhillips
600 N Diary Ashford Street,
Houston, TX-77079

Email Address: happymanan@gmail.com

Education: B.S., Information and Computing Science, China University of Petroleum Beijing, China (2007)

M.S., Geophysics, Texas A & M University, College Station, TX (2009)